

Facies architecture, geochemistry and petrogenesis of Middle Triassic volcanoclastic deposits of Mt. Ivanščica (NW Croatia): evidence of bimodal volcanism in the Alpine-Dinaridic transitional zone

Smirčić, Duje; Vukovski, Matija; Slovenec, Damir; Kukoč, Duje; Šegvić, Branimir; Horvat, Marija; Belak, Mirko; Grgasović, Tonći; Badurina, Luka

Source / Izvornik: **Swiss Journal of Geosciences, 2024, 117**

Journal article, Published version

Rad u časopisu, Objavljena verzija rada (izdavačev PDF)

<https://doi.org/10.1186/s00015-024-00453-8>

Permanent link / Trajna poveznica: <https://urn.nsk.hr/urn:nbn:hr:169:417052>

Rights / Prava: [Attribution 4.0 International](#)/[Imenovanje 4.0 međunarodna](#)

Download date / Datum preuzimanja: **2025-03-14**



Repository / Repozitorij:

[Faculty of Mining, Geology and Petroleum Engineering Repository, University of Zagreb](#)




ORIGINAL PAPER

Open Access



Facies architecture, geochemistry and petrogenesis of Middle Triassic volcanoclastic deposits of Mt. Ivanščica (NW Croatia): evidence of bimodal volcanism in the Alpine-Dinaridic transitional zone

Duje Smirčić¹, Matija Vukovski², Damir Slovenec^{2*} , Duje Kukoč², Branimir Šegvić³, Marija Horvat², Mirko Belak², Tonči Grgasović² and Luka Badurina^{3,4}

Abstract

During the Middle Triassic, intensive volcanic activity took place along the eastern margin of Pangea, including the Greater Adria promontory, due to the Neotethyan oceanization. This resulted in the formation of various volcanic and volcanoclastic rock types. The region of NW Croatia, acting as a transition zone between the Southern Alps and the Dinarides, showcases the outcrops of these rocks. The present study investigates the facies of volcanoclastic rocks, the distribution of those facies, formation processes, as well as the genesis of the primary magma to gain a better understanding of the complex geodynamics of this region during the Middle Triassic. Six profiles across the Vudelja quarry front were surveyed using drone imaging and samples were collected for detailed petrographic and geochemical analyses. Two groups of volcanoclastic rocks were identified—*mafic* and *intermediate/felsic*. The former is represented by (I) autoclastic effusive facies and (II) resedimented autoclastic facies, while the latter is represented by (III) secondary pyroclastic facies. Mafic volcanoclastics were generated through basaltic effusions in marine environments, fragmentation in contact with seawater, mixing with shallow marine carbonate clasts, and subsequent redeposition in deeper marine areas. The secondary pyroclastic facies (III) consists of a regionally distributed felsic *Pietra Verde* tuff whose deposits may be related to pyroclastic density currents and syn-eruptive resedimentation by turbidite-like currents. Geochemical data indicate that parental magmas responsible for generating the mafic volcanoclastics had a calc-alkaline composition and originated in ensialic and mature arc settings of an active continental margin. The observed chemical composition is likely inherited from older, arc-related lithologies, associated with the subduction of the Paleotethys Ocean. Parental magmas are thought to have formed during continental rifting of the passive Middle Triassic margins of the Greater Adria through (i) partial melting of the heterogeneous lithospheric mantle, which had been metasomatized during an earlier Hercynian subduction, and (ii) subordinate processes related to the melting of the upper continental crust and subsequent fractionation. Ar/Ar dating on plagioclase separates yielded an age of 244.5 ± 2.8 Ma for mafic volcanoclastics. This aligns well with biostratigraphic ages of felsic tuffs which crop out on a broader regional scale of the Dinarides, the Southern Alps, and the Transdanubian Range. The overlapping

Editorial handling: Boštjan Rožič

*Correspondence:

Damir Slovenec

dslovenec@hgi-cgs.hr

Full list of author information is available at the end of the article



© The Author(s) 2024. **Open Access** This article is licensed under a Creative Commons Attribution 4.0 International License, which permits use, sharing, adaptation, distribution and reproduction in any medium or format, as long as you give appropriate credit to the original author(s) and the source, provide a link to the Creative Commons licence, and indicate if changes were made. The images or other third party material in this article are included in the article's Creative Commons licence, unless indicated otherwise in a credit line to the material. If material is not included in the article's Creative Commons licence and your intended use is not permitted by statutory regulation or exceeds the permitted use, you will need to obtain permission directly from the copyright holder. To view a copy of this licence, visit <http://creativecommons.org/licenses/by/4.0/>.

ages obtained from radiometric dating of mafic volcanoclastics and biostratigraphic ages of the felsic *Pietra Verde* tuffs strongly suggest that the Greater Adria region experienced concurrent bimodal volcanism during the Middle Triassic.

Keywords Autoclastic deposits, Pyroclastic deposits, Active continental margin, Mt. Ivanščica, Croatia, Middle Triassic

1 Introduction

The Middle Triassic volcano-sedimentary successions in NW Croatia are cropping out in the intra-Pannonian Mountain chain extending for 60 km in the east–west direction (Fig. 1A, B). These mountains, regarded as the southernmost part of the Southern Alps (*sensu* Schmid et al., 2008, 2020), are located in a tectonically complex area at the contact with the Dinarides. The occurrences of Middle Triassic volcanic, volcanoclastic, and sedimentary rocks are spatially and genetically linked to rifting processes related to the initiation of the Maliak-Meliata-Vardar branch of the Neotethys Ocean (*sensu* Schmid et al., 2008, 2020). Stratigraphically correlative successions are well known from the Southern Alps, the Dinarides and the Transdanubian Range (Castellarin et al., 1988; De Zanche et al., 1993; Gianolla et al., 1998; Goričan et al., 2005; Smirčić et al., 2018, 2020a; Haas & Budai, 1995; Harangi et al., 1996; Velledits, 2004, 2006; Budai & Vörös, 2006; Velledits et al., 2017), however, their geodynamic evolution has not yet been unambiguously resolved. Previous studies have not been conclusive on the origin of Middle Triassic magmatism, which has been commonly associated with continental rifting (Pamić, 1984; Crisci et al., 1984; Pamić & Balen, 2005; Del Piaz & Martin, 1998; Knežević et al., 1998; Aljinović et al., 2010; Bortolotti et al., 2013; Saccani et al., 2015; De Min et al., 2020). Alternatively, it may be related to convergent plate movements caused by the subduction of the Paleotethys Ocean (Bébian et al., 1978; Castellarin et al., 1980, 1988; Obenholzer, 1991; Bonadiman et al., 1994; Trubelja et al., 2004; Stampfli & Borel, 2002, 2004; Schmid et al.,

2004; Grimes et al., 2015; Smirčić et al., 2018; Casetta et al., 2018; Bianchini et al., 2018; Storck et al., 2018; Slovenec et al., 2020, Slovenec & Šegvić, 2021, Slovenec et al., 2023a and b). Considering the complex magmatic activity in the western part of the Neotethys Ocean and related geodynamic processes along its margins, the research of volcanic and volcano-sedimentary successions represents a valuable source of information and is of key importance to unveil multiple lithospheric processes in such a geodynamic environment (Lustrino et al., 2019, Storck et al., 2020).

The study area is located on the slopes of Mt. Ivanščica, one of the intra-Pannonian mountains, where igneous and volcanoclastic rocks were documented by Golub & Brajdić (1970), Marci et al. (1982, 1984), and Goričan et al. (2005). Recent research of upper Anisian volcano-sedimentary successions in the eastern part of Mt. Ivanščica reports on the origin, geodynamic significance, and diagenetic/hydrothermal history of volcanic/volcanoclastic rocks and associated cherts (Slovenec et al., 2020; 2023b; Slovenec & Šegvić, 2021; Šegvić et al., 2023).

The formation processes, emplacement mechanisms, petrogenesis, as well as tectonic setting of mafic volcanoclastic deposits from the northern part of Mt. Ivanščica are studied by analyzing their sedimentological, mineralogical, petrological, and geochemical features. In this paper we utilize isotope and paleontological data, along with structural characteristics, to determine the stratigraphical position of mafic volcanoclastic deposits within the Triassic period. Finally, this contribution provides new data that will help in our understanding

(See figure on next page.)

Fig. 1 **A** Geotectonic sketch map of the major tectonic domains (simplified after Schmid et al., 2008). **B** Geological sketch map of the Croatian part of the Zagorje-Mid-Transdanubian Zone, i.e. Sava Composite Unit (slightly modified after Pamić & Tomljenović, 1998 and Haas et al., 2000). Legend: 1 = Quaternary and Neogene fill of the Pannonian Basin; 2 = Upper Cretaceous–Paleocene flysch; 3 = Ophiolitic mélangé (Kalnik Unit); 4 = Upper Triassic platform carbonates; 5 = Upper Paleozoic and Triassic clastics and carbonates interlayered with volcanics and tuffs; 6 = Paleozoic–Triassic metamorphic complex (Medvednica Unit). **C** Simplified geological sketch map of the central part of Ivanščica Mt. (modified after Šimunić et al., 1982). Legend: 1—Neogene and Pleistocene sedimentary rocks; 2—Upper Jurassic–Lower Cretaceous limestones, shales, cherts, 3—Jurassic ophiolite mélangé with blocks of basalt and gabbro (blue field), 4—Upper Triassic limestones, dolomites and dolomite breccias, 5—Upper to Middle Triassic dolomites, dolomite breccias and limestones, 6—Middle to Lower Triassic dolomites, limestones, dolomite breccias, radiolarites, clastics rocks intersected by a series of andesite-basalts (dark green field) and/or acid tuffs (light green field); 7—reverse or thrust faults; 8—normal faults; 9—discordance line, tectonic-erosion discordance; 10—sample location. **D** Detailed geological map of the study area compiled from Šimunić et al. (1982) and the results of this study. **a** Stereoplot of bedding planes (purple lines) and fold axes (F) measured in Lower Triassic sediments of the Vilinska špica nappe and bedding planes measured in Middle Triassic volcanoclastic rocks from the footwall (black lines). **b** Stereoplot of bedding planes (black lines), fault planes (red lines) and fold axis (F) measured in Middle Triassic volcanoclastic rocks from the Vudelja Quarry. **(c)** Stereoplot of the bedding planes measured in Middle Triassic sediments (black lines) and Lower Miocene sediments (blue lines) and the fault planes measured in Middle Triassic sediments (red lines)

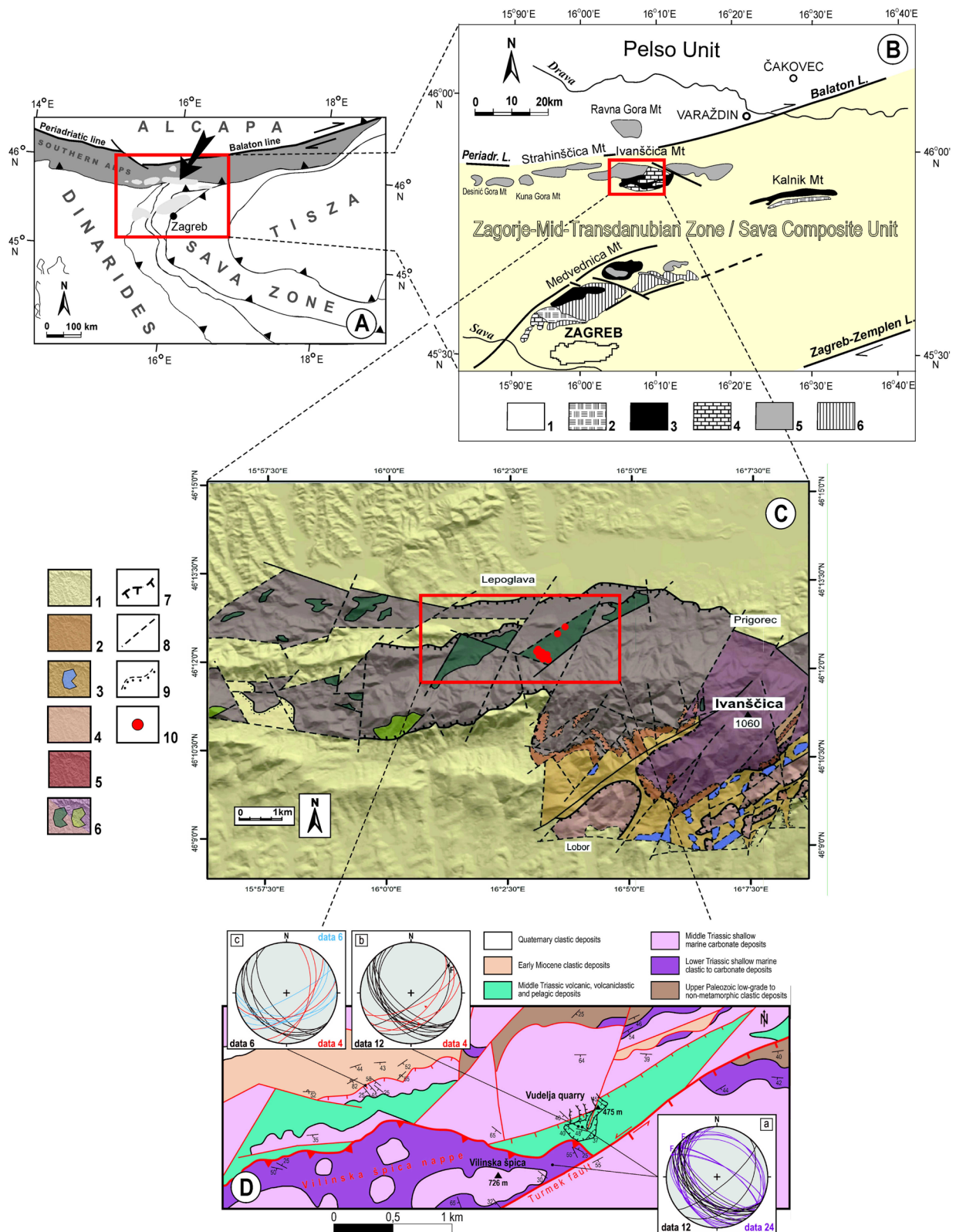


Fig. 1 (See legend on previous page.)

of geodynamic events occurring at the margin of the Greater Adria Plate (sensu van Hinsbergen et al., 2020) during the early evolution of the Neotethys Ocean in the Middle Triassic.

2 Geological setting

In northwest Croatia, several mountains expose Mesozoic igneous and volcanoclastic rocks of ophiolitic and continental margin origin (Fig. 1A, B). These mountains, including Mt. Ivanščica, are found in the SW segment of the Sava Composite Unit (sensu Haas et al., 2000) or the Zagorje-Mid-Transdanubian shear Zone (ZMTDZ; sensu Pamić & Tomljenović, 1998; Fig. 1B). The latter is situated south of the ALCAPA (Alpine-Carpathian-Pannonian) Mega-Unit and between the two regional fault systems: the Zagreb-Zemplen Line to the south and the Periadriatic-Balaton Line to the north and was derived from continental crustal domains containing ophiolites previously obducted on the continental margin (Harangi et al., 1996; Haas & Kovács, 2001).

According to Schmid et al. (2008, 2020), Mt. Ivanščica is considered a part of the Southern Alps and is located in close proximity to the Internal Dinarides. In the wider study area, originally NW–SE trending Dinaridic structures were rotated clockwise during the Oligocene – earliest Miocene (Tomljenović et al., 2008), and overthrust in the Miocene by the S-verging frontal thrust of the South Alpine unit (van Gelder et al., 2015; Schmid et al., 2008, 2020). From the Late Miocene to the present day this area was finally folded and rotated counterclockwise (Tomljenović and Csontos, 2001; Tomljenović et al., 2008). Consequently, in the wider study area present day Dinaridic structures deviate from their original orientation and exhibit NW vergence and NE-SW orientation overprinted by younger S-SW vergent Alpine structures (van Gelder et al., 2015; Schmid et al., 2008, 2020). Both tectonic units, however, share a common paleogeographic origin, the eastern continental margin of the Adria microplate (van Hinsbergen et al., 2020).

Middle Triassic shallow to deep-marine successions consisting of volcanic and volcanoclastic rocks intercalated within marine sedimentary rocks are preserved on Mt. Ivanščica (e.g., Goričan et al., 2005; Slovenec et al., 2020, 2023b; Kukoč et al., 2023). These volcanosedimentary successions were deposited in a relatively short-lived basin, the Northwestern Croatian Triassic Rift Basin (NCTRB; Kukoč et al., 2023) formed on the Adriatic continental margin due to rifting-related extension. The northern slopes of Mt. Ivanščica (Fig. 1C) feature volcanic and volcanoclastic rocks with a wide range of compositions, including basic, intermediate, and acidic effusive and volcanoclastic

lithologies. These rocks are interbedded with Middle Triassic marine deposits consisting of siliceous (radiolarite) and carbonate (limestone, dolostone) lithologies (e.g., Šimunić & Šimunić, 1979, 1997; Marci et al., 1982, 1984; Šimunić, 1992; Goričan et al., 2005; Slovenec et al., 2020, 2023b; Kukoč et al., 2023). The Middle Triassic volcanism developed through submarine calc-alkaline basaltic to andesitic lava flows accompanied by multiple explosive eruptions of volcanoclastic material and interpreted as remnants of a late Anisian-Ladinian volcanic arc (Goričan et al., 2005; Slovenec et al., 2020, 2023b; Slovenec & Šegvić, 2021; Kukoč et al., 2023). These Middle Triassic successions on Mt. Ivanščica are overlain by the shallow marine to pelagic successions spanning from the Late Triassic to the Early Cretaceous (Babić, 1974; Vukovski et al., 2023; Fig. 1C). Sedimentary successions of Mt. Ivanščica are thrust southwards onto the Neotethys stemmed ophiolite mélange during the Neogene (van Gelder et al., 2015; Schmid et al., 2008, 2020; Fig. 1C).

The studied volcanoclastic rocks crop out in a 2 km long and 300 m wide, NE-SW striking continuous belt, which tends to extend further to the west where is more discontinuous and tectonically dissected (Fig. 1D). The estimated thickness of the investigated volcanoclastic rocks is more than 100 m. The northern boundary of the volcanoclastic rocks has only partially preserved primary sedimentological contact with underlying Middle Triassic carbonates, while the rest of the contact is characterized by minor faulting. The southern boundary of the volcanoclastic belt is a major thrust fault that brings in contact volcanoclastic rocks with Lower to Middle Triassic shallow to deep-marine successions of the overlying tectonic unit, informally named the Vilinska Špica nappe (Fig. 1D). The Turmek fault, representing south-eastern border of the studied volcanoclastic belt, juxtaposes Middle Triassic volcanoclastic rocks and slightly older Middle Triassic shallow-marine reefal limestones (Fig. 1D). Dominantly SW-ward dipping beds in volcanoclastic rocks are overlain by Lower to Middle Triassic sediments with dominantly SW-ward dipping bedding planes (Fig. 1D).

In the wider area a large volume of Middle Triassic mafic volcanoclastic deposits, interlayered with rare felsic tuffs are recorded. These rocks are found exclusively in the footwall of the Vilinska Špica nappe. On the other hand, within the succession of the Vilinska Špica nappe, felsic tuffs, commonly referred to as *Pietra Verde*, alternate with deep-marine sedimentary lithologies with scarce intercalations of mafic volcanoclastic deposits (Slovenec et al., 2023b; Kukoč et al., 2023).

3 Materials and analytical techniques

The volcanoclastic, pyroclastic, and associated carbonate rocks investigated in this study are situated in the broader area of the Vudelja Quarry, located on the northern slopes of Mt. Ivanščica (Fig. 1C, D). To ensure accurate documentation, the quarry front was scanned and photographed using a drone. The resulting image was then referenced, enabling the precise plotting of all collected samples (Fig. 2). The quarry front is heavily covered by talus and scree which makes contouring of distinct facies complicated. Therefore, the zonation of the facies was limited only to the vicinity of the collected samples where the outcrops were clear of cover.

For this research samples were collected from six geological profiles (profiles are named: VU I, VU II, VU III, VU IV, VU V, VU VI; Fig. 2) with 62 representative samples chosen for further study. Macroscopic and microscopic observations were performed to determine petrographical features of rocks. Microscopic observations were done on Olympus BH-2 and Zeiss Axio Lab. A1 microscopes equipped with a digital camera (Croatian Geological Survey Zagreb, Croatia) and Optika B 1000 POL polarizing microscope and Optika C-P6 FL camera of the University of Zagreb, Faculty of Mining, Geology and Petroleum Engineering (Zagreb, Croatia). Volcanoclastic facies were determined based on the

classifications of Fisher (1961), McPhie et al. (1993), White & Houghton (2006), and Di Capua et al. (2022).

Mineral compositions of two representative samples were analysed at the University of Geneva, Department of Earth Sciences (Geneva, Switzerland) using a JEOL JXA 8200 Superprobe (JEOL Ltd., Akishima, Japan) electron microprobe equipped with a wavelength/energy dispersive combined microanalyzer. Operating parameters included an accelerating voltage of 20 kV, a 20 nA beam current, and a beam size of $\sim 1 \mu\text{m}$ (for feldspars $10 \mu\text{m}$). Counting times of 20 s on peak and 10 s on background on both sides of the peak were used for all elements. Limits of detection (LOD) were calculated as the minimum concentration required to produce count rates three times higher than the square root of the background (3σ ; 99 wt.% degree of confidence at the lowest detection limit). Concentrations below the LOD are reported as not detected. Raw data were corrected for matrix effects using the PAP algorithm implemented by JEOL (Pouchou & Pichoir, 1984, 1985). Natural minerals, oxides (corundum, spinel, hematite, and rutile), and silicates (albite, orthoclase, anorthite, and wollastonite) were used for calibration. Mineral formulas were calculated using a software package MINPET written by Linda R. Richard (Gatineau, Québec, Canada).

XRF was utilized to acquire the whole-rock geochemistry of collected samples, which were first crushed

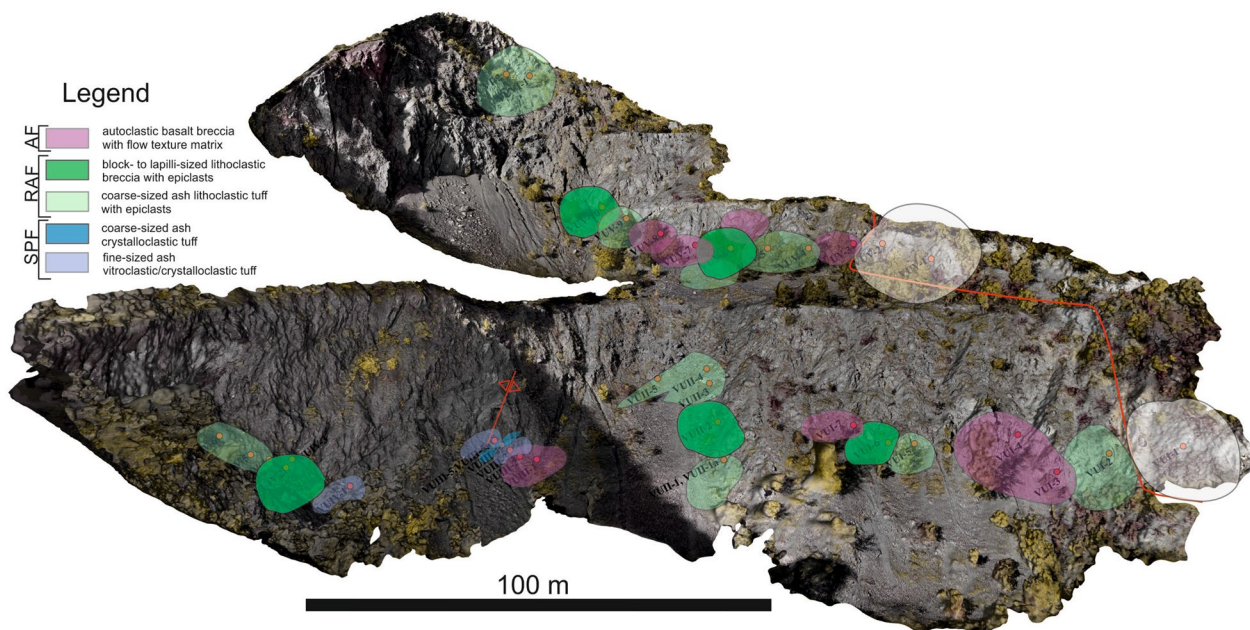


Fig. 2 A drone image of the quarry front with sample positions. Different colours represent different facies and pertaining lithotypes. AF—Autoclastic effusive facies presented by the lithotype of autoclastic basalt breccia with flow texture matrix containing clasts of several different basalts. RAF—Resedimented autoclastic facies with two different lithotypes: block to lapilli-sized basalt breccia with epiclasts, and coarse-sized ash lithoclastic tuff. SPF—Secondary pyroclastic facies with three different lithotypes: (1) coarse-sized ash lithoclastic tuff, (2) fine-sized ash crystalloclastic tuff and (3) fine-sized ash vitroclastic/crystalloclastic tuff. General coordinates of the quarry $16^{\circ}3'21.42''\text{E}$; $46^{\circ}11'41.42''\text{N}$. Graphical scale is indicated in the figure

with a mortar and pestle into a fine powder and then mixed with $\text{Li}_2\text{B}_4\text{O}_7$ in 1:5 ratio. Samples were subjected to loss of ignition treatment which included heating at 1000 °C for 30 min and subsequent fusion. XRF data were collected on fused glass discs using Thermo Scientific ARL Perform'X sequential and U.S. Geological Survey standards. Trace-element abundances in glass discs previously used for XRF measurements were collected using an Agilent 7500cs quadrupole mass spectrometer equipped with a New Wave UP-213 solid state laser with dual-volume cell. The laser was operated at a frequency of 15 Hz, a spot size of 100 μm and a measured fluence of between 6 and 7 Jcm^{-2} . The GSD-1G glass and Si abundances from XRF analyses were used as external and internal standards, respectively. The US Geological Society rock standard BHVO-2G (Jochum et al., 2005) served to monitor instrument performance, precision, and accuracy. Major element and trace element concentrations were measured with accuracy and precision better than $\pm 1\%$ and $\pm 5\%$, respectively. It is 3σ at 10 times the detection limit. The quality of the measurements was checked by replicating the analysis on $\sim 12\%$ of the samples. Both XRF and LA-ICP-MS analyses were carried out at GeoAnalytical Laboratory of Texas Tech University Department of Geosciences (Lubbock TX, USA).

Nd isotopic compositions of three bulk rock samples were measured at the Noble Gas Laboratory Pacific Centre for Isotopic and Geochemical Research, University of British Columbia, Vancouver (Canada) using a Triton Plus mass spectrometer. Normalizing ratios of $^{146}\text{Nd}/^{144}\text{Nd}=0.7219$ were assumed. The $^{143}\text{Nd}/^{144}\text{Nd}$ ratio for the La Jolla standard was 0.5118451 ± 0.000010 (2σ). Total procedural blanks were ~ 150 pg. Python™ programming language (numpy package) was used to calculate the Monte Carlo propagation error through 10000 iterations for $^{143}\text{Nd}/^{144}\text{Nd}_{(t)}$.

X-ray diffraction (XRD) was carried out on a set of four representative samples. For that purpose, the material was firstly gently crushed and powdered in an agate mortar and was thereupon placed in the sample holder. The material was analysed with a Bruker D8-Advanced diffractometer installed at Texas Tech Department of Geosciences (Lubbock TX, USA) using a step scan mode in the Bragg–Brentano geometry with $\text{CuK}\alpha$ radiation. The measurement settings were 45 kV and 40 mA with sample mounts scanned from 3 to 70 $^\circ 2\theta$ at a counting time of 2.5 s per 0.02 $^\circ 2\theta$. The Bruker EVA diffraction suite and the Powder Diffraction File 4 issued by the International Centre for Diffraction Data were used to analyze the diffraction data. Lastly, XRD traces were, once interpreted, compared with the whole-rock geochemistry generated from LA-ICP-MS to ensure geological fluidity.

Plagioclase separate from basaltic volcanoclastic (sample VU II-1) was separated by electromagnetic separator and standard heavy liquid techniques and finally was purified by hand picking under binocular lenses. The plagioclase separate was wrapped in Al foil and stacked in an irradiation capsule with similar-aged samples and neutron flux monitors (Fish Canyon Tuff sanidine), 28.201 ± 0.046 Ma (Kuiper et al., 2008). Samples were irradiated at the McMaster Nuclear Reactor (Hamilton ON, Canada) and analysed at the Noble Gas Laboratory Pacific Centre for Isotopic and Geochemical Research, University of British Columbia (Vancouver BC, Canada). The mineral separates were step-heated at incrementally higher powers in the defocused beam of a 10W CO_2 laser (New Wave Research MIR10) until fused. The gas evolved from each step was analysed by a VG5400 mass spectrometer equipped with an ion-counting electron multiplier. All measurements are corrected for total system blank, mass spectrometer sensitivity, mass discrimination, radioactive decay during and subsequent to irradiation, as well as interfering Ar from atmospheric contamination and the irradiation of Ca, Cl and K (Isotope production ratios: $(^{40}\text{Ar}/^{39}\text{Ar})_{\text{K}}=0.0302 \pm 0.00006$, $(^{37}\text{Ar}/^{39}\text{Ar})_{\text{Ca}}=1416.4 \pm 0.5$, $(^{36}\text{Ar}/^{39}\text{Ar})_{\text{Ca}}=0.3952 \pm 0.0004$, $\text{Ca}/\text{K}=1.83 \pm 0.01(^{37}\text{Ar}_{\text{Ca}}/^{39}\text{Ar}_{\text{K}})$). Initial data entry and calculations were carried out using the software ArArCalc (Koppers, 2002). The plateau and correlation ages were calculated using ISOPLOT ver. 3.09 (Ludwig, 2003). Errors are quoted at the 2σ (95% confidence) level and are propagated from all sources except mass spectrometer sensitivity and age of the flux monitor.

4 Volcanoclastic facies determination

Four facies were determined:

(I) *Autoclastic effusive facies (AF)*.

Samples belonging to this facies are shown in Fig. 2 and Table 1. Rocks of the AF are presented by a very poorly sorted, mostly matrix supported basaltic breccias with carbonate epiclasts – *autoclastic basalt breccia*. The size of basaltic lithoclasts varies (Table 1). Clasts are largely irregular in shape (Table 1; Fig. 3A). Several types of basalt clasts are determined (Table 1):

- (a) Basalt clasts composed of hyaline matrix and plagioclase phenocrysts. Altered plagioclase phenocrysts reach up to 0.8 mm in size (Table 1). Rare pyroxene phenocrysts reach up to 1.5 mm in size and are thoroughly altered to oxide minerals and chlorite-like phases (Table 1). The latter is referred to as chlorite in the following text. This basalt clast type typically has amygdaloidal vesicles filled with fan-like aggregates of chlorite, calcite, and dolomite.

Table 1 Synthetic table of the determined volcanic facies and lithotypes in the Vudolja Quarry with their petrographical and mineralogical characteristics

Facies	Lithotype	Texture	Structure	Particle size	Volcanic lithoclasts	Crystalloclasts	Vitroclasts	Epiclasts	Matrix	Alteration products	Chemical composition
(I) <i>Autoclastic effusive facies (AF)</i>	<i>Basalt breccia with carbonate epiclasts</i>	Chaotic	Very poorly sorted; Matrix supported; Very coarse clasts dominate, irregular, elongated, subrounded to blocky	Coarse ash to block size	(a) Porphyre/ glomeroporphyre amygdaloid basalts with plagioclase phenocrystals; (b) aphyric amygdaloid basalts; (c) porphyritic olivine basalts with plagioclase glomeroporphyric clusters; (d) basalts with crystallized matrix composed of needle like plagioclase, pyroxene, chlorite, and epidote	Idiomorphic to hypidiomorphic pyroxene; idiomorphic to hypidiomorphic plagioclase	–	Micritic limestone with pelagic fossils; intra-clast packstone skeletal grainstone, dolostromatolite; Limestone containing shallow marine fossils	Hyaline with flow texture, curvature around the clasts and alignment of fine needle-like plagioclase microliths	Plagioclase altered to calcite, prehnite, clay minerals, sericite; Pyroxene altered to chlorite and opaque minerals; Olivine altered to fibrous serpentine aggregates	Mafic
(II) <i>Resedimented autoclastic facies (RAF)</i>	<i>Lapilli-sized basalt breccia with epiclasts</i>	Rare normal grading; sometimes interlayered with coarse-sized ash lithoclastic tuff	Poorly sorted; Matrix to clast supported; Coarse clasts, irregular, subrounded to rounded	Coarse ash to lapilli size	Basaltic lithoclasts as above; Fine ash vitroclastic tuff	Idiomorphic to irregular plagioclase; very small needle-like pyroxene	Scoria fragments	Micritic limestone with pelagic fossils	Dark brown/ green sedimentary type matrix of very fine hyaline clasts, crystalloclasts and scoria fragments prevailing over chlorite/ calcite cement	Plagioclase altered to calcite and prehnite; Pyroxene altered to chlorite and opaque mineral aggregates	Mafic
	<i>Coarse-sized ash lithoclastic tuff</i>	Common normal grading; sometimes interlayered with lapilli-sized basaltic breccia with epiclasts	Well sorted; Clast supported; subrounded to rounded	Coarse ash size	Basaltic lithoclasts as above; composition of clasts not recognizable due to their relatively small size	Idiomorphic to allotropic plagioclase with lamellar texture, when fragmented Jig-saw fit texture; idiomorphic to hypidiomorphic K-feldspar; fragmented quartz	Pumice fragments	Micritic limestone with pelagic fossils and biosparite/biomicroite limestone	Very fine-grained dark matrix and calcite cement	Plagioclase altered to calcite, prehnite and opaque mineral aggregates; K-feldspar to clay minerals and fine-grained mica; Pumice fragments devitrified to chlorite and microcrystalline quartz	

Table 1 (continued)

Facies	Lithotype	Texture	Structure	Particle size	Volcanic lithoclasts	Crystalloclasts	Vitroclasts	Epiclasts	Matrix	Alteration products	Chemical composition
(//) Secondary pyroclastic facies (SPF)	Coarse-sized ash crystalloclastic tuff	Strong imbrication of elongated clasts	Moderately sorted; Flow banded pumice around the crystalloclasts	Coarse ash to lapilli size	Basaltic lithoclasts of serrated shape	idiomorphic to hypidiomorphic zonal plagioclase	Pumice fragments; glass shards	–	Volcanic glass devitrified to chlorite	Plagioclase altered to prehnite and calcite; Pumice fragments to chlorite	Intermediate/Felsic
	Fine ash crystalloclastic tuff	Horizontal to wavy lamination; interlayered with the following unit	Very well sorted	Fine-sized ash	Basaltic lithoclasts	Irregularly shaped quartz; idiomorphic to hypidiomorphic K-feldspar and plagioclase	Fine glass shards	–	Calcite cement or very fine dark matrix	K-feldspar and plagioclase altered to clay minerals; fine-grained mica, prehnite and calcite aggregates	Felsic
	Fine ash vitroclastic tuff	Horizontal to wavy lamination; interlayered with the former unit	Very well sorted	Very fine- to fine-sized ash	–	–	Very fine glass shards	–	Very fine dark matrix	Glass shards devitrified to chlorite	

- (b) Aphyric basalt lithoclasts with amygdaloid vesicles. Vesicles are filled with chlorite, epidote, and calcite. A faint and unclear alignment of amygdales is documented in some of these lithoclasts. Exceptionally rare crystallites of plagioclase and pyroxene were determined.
- (c) Clasts of olivine basalt with porphyritic texture composed of dark brown hyaline matrix with plagioclase and olivine phenocrystals (Table 1).
- (d) Clasts showing slightly porphyritic texture with microcrystalline groundmass. The discriminant characteristic of this lithoclast type is the presence of a crystallized matrix (Table 1). The elongated minerals exhibit imbrication patterns. These clasts also have a certain number of amygdales filled with fan-shaped chlorite aggregates and calcite. Rare plagioclase and pyroxene phenocrystals are completely altered (Table 1).

The basaltic lithoclast component occupies around 70 vol.% of the rocks from this facies (Fig. 3A). The second most common constituent of this facies are crystalloclasts up to 1 mm in size (Table 1).

Epiclasts determined in this facies are presented by carbonates (Fig. 3A). Two types of carbonate clasts can be distinguished – dolostone and limestone (Table 1). Fossils of encrusting organisms were noticed in the limestone clasts and are determined as *Plexoramea cerebriformis* MELLO and *Olangocelia otti* BECHSTADT & BRANDNER (Fig. 3B). These fossil assemblages are typical of Middle Triassic reefs. *Olangocelia otti* is determined as a typical Anisian species (Senowberi-Daryan et al., 1993), while *Plexoramea cerebriformis* ranges from the Pelsonian to the Carnian.

The matrix, composed of hyaline substrate, is characterized by a strong dominance of foliation seen as irregular linear spread between the clasts (Fig. 3C). In some places small microliths can be seen in the matrix contributing to the foliation. The curvature of the matrix may be aligned around the clasts, indicating a flow texture matrix (Fig. 3C). Subordinately, the chlorite cement may also be recognized, and is composed of fine chlorite aggregates with needle-like plagioclase microliths organized in faint imbrication patterns (Fig. 3D).

(II) *Resedimented autoclastic facies (RAF)*.

Rocks of this facies are presented by two different lithotypes based on the clasts size as well as the rocks' composition, structure, and texture (Table 1).

The first lithotype is determined by lapilli-sized volcanic clasts and ~30 vol.% of carbonate epiclasts – *block-to lapilli-sized basalt breccia with epiclasts* (Table 1, Fig. 2). Clasts found in this lithotype are very irregular

in shape. Granulometric bimodality is recognized with lapilli-sized clast mostly supported by dark brown to dark green to black matrix. The composition of clasts in the samples of this lithotype is similar to the aforementioned *autoclastic effusive facies* (Table 1). One specific lithoclast type observed in this lithotype is composed of entirely chloritized fine ash vitroclasts (Table 1; Fig. 3E). Horizontal lamination has sporadically been documented in such clasts. These clasts belong to felsic fine ash vitroclastic tuffs described in detail in the upcoming *secondary pyroclastic facies*. The main difference that allowed the distinction of RAF from the aforementioned AF is the presence of a sedimentary-type matrix and cement (Table 1). The matrix is composed of very fine volcanic particles (Fig. 3F). In addition to the matrix, a smaller quantity of chlorite or calcite cement can also be observed (Table 1; Fig. 3G).

The second lithotype within the RAF is distinguished by its variation in grain size and is referred to as *coarse-sized ash lithoclastic tuff* (Table 1, Fig. 2). The samples are characterized by very good sorting and occasionally a grading texture with gradual transitions from the *lapilli-sized basalt breccia with epiclasts* (Fig. 3H). Clasts are dominantly made of lithoclasts of various volcanic effusive rocks (Table 1). The presence of crystalloclasts is more abundant in this lithotype than in the one previously described (Fig. 3F). The most common type of crystalloclasts is plagioclase (Table 1). K-feldspars are found in smaller quantities (Table 1, Fig. 3G), while quartz crystalloclasts are the least abundant (Table 1). About 5% of clasts are represented by elongated pumice fragments (Table 1). The clasts in this lithotype feature point-to-line contacts, with varying pore spaces from 5 to 20%. Pore space between the clasts is filled either by a very fine-grained dark matrix or by calcite cement (Fig. 3G).

(III) *Secondary pyroclastic facies (SPF)*.

Deposits of the SPF are presented by three different lithotypes: (1) *coarse-sized ash crystalloclastic tuff*; (2) *fine-sized ash crystalloclastic tuff* and (2) *fine-sized ash vitroclastic tuff* (Table 1).

The first lithotype was determined in one sample only (VU III-4). This sample exhibits a pronounced imbrication of elongated clasts (Table 1; Fig. 3I). The dominant constituents of this lithotype are plagioclase crystalloclasts (Table 1). Some crystalloclasts are coated by a thin envelope of dark volcanic glass. Elongated pumice fragments are also present (Fig. 3I). They range from 1 to 2 mm in size (Table 1). Some pumice fragments show ductile deformations in contact with crystalloclasts. Basalt lithoclasts occupy around 10 vol.% of the sample (Table 1). Matrix is composed exclusively of secondary chlorite (Fig. 3I).

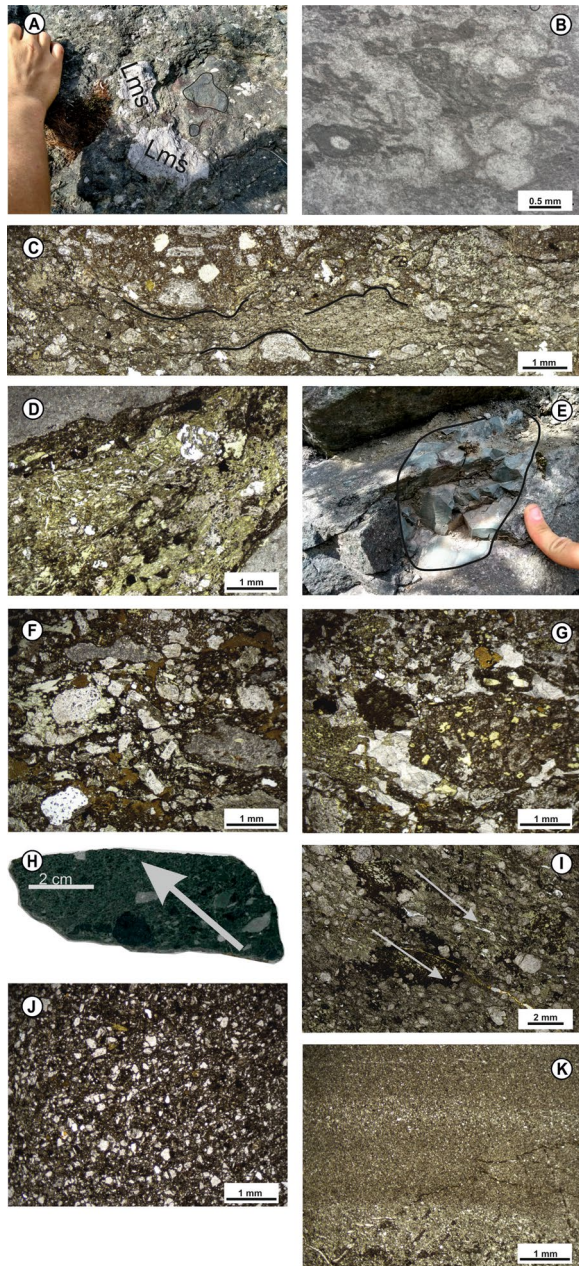


Fig. 3 Petrographic characteristics of the described facies. **A** Field photograph of the autoclastic basalt facies outcrop. Some basalt clasts are outlined in dark. Notice also the hand sized limestone clasts (Lms). The rocks are very chaotic and poorly sorted. **B** Fossils of *Plexoramea cerebriformis* MELLO and *Olangocoelia otti* BECHSTÄDT and BRANDNER from limestone clast found in the *autoclastic basalt facies*, sample VU II-2A. **C** A stitched microphotograph exhibiting flow texture matrix between the basalt lithoclasts. The matrix area is outlined with dark lines. In the lower middle part of the photograph the matrix is rounding the plagioclase crystalloclast – sample VU I-4a. **D** Between the clasts in the *autoclastic basalt facies* chlorite cement is seen with small needle like crystals of plagioclase – sample VU III-1. **E** Clasts of vitroclastic tuffs seen in the *resedimented autoclastic facies*. The clasts are outlined in the field photograph. **F** Photomicrograph of the *lapilli-sized basalt breccia with epiclasts* from the *resedimented autoclastic facies* (sample VU V-10). Notice that the matrix is composed of finely fragmented volcanic particles. Clasts are very irregular. The amount of the crystalloclastic particles is more abundant in this facies. **G** The same lithotype of the same facies but with different material in the pore spaces between the clasts (sample VU V-6a). Here the unsorted and irregular clasts mostly of different types of basalts are cemented by calcite cement. **H** A scanned polished sample VU IV-6 of the *resedimented autoclastic facies* exhibiting grading texture indicated by the arrow. Grading texture results in the transition from *lapilli-sized basalt breccia* to the *coarse-sized ash lithoclastic tuff* that is composed mostly of basalt clasts. **I** Photomicrograph of the *coarse ash crystalloclastic tuff* of the *secondary pyroclastic facies* composed mostly of plagioclase crystalloclast, and vitric particles. Notice the vesicular rich particles of dark pumice fragments. The whole sample exhibits a strong imbrication pattern of particles indicated by the grey arrows – sample VU III-4. **J** *Fine ash crystalloclastic tuff* of the *secondary pyroclastic facies* composed mostly of crystalloclasts (VU III-6c). Notice the abundance of quartz crystalloclast in this facies indicating the acidic origin of the pyroclastic material. Also seen from the geochemical analysis. **K** *Fine ash vitroclastic tuff* with horizontal lamination from the *secondary pyroclastic facies* composed of very fine glass shards barely visible with the polarizing microscope (sample VU III-6)

Fine-sized ash vitroclastic tuff is composed of densely packed very fine to fine glass shards (Fig. 3K; Table 1). Their shapes are not clearly distinguishable due to their small size. The entire lithotype exhibits a greenish coloration due to the devitrification process (Table 1). The predominant feature of the entire facies is the presence of horizontal to wavy lamination (Fig. 3K). In places, the two lithotypes alternate within the laminae.

Samples from the other two lithotypes are combined into one group in Fig. 2 and are marked as VU III-3, VU III-5, VU III-5a, and VU IV-1. *Fine-sized ash crystalloclastic tuff* is composed dominantly of crystalloclasts (Fig. 3J; Table 1). A certain number of lithoclasts (up to 40 vol.%) is also present (Fig. 3J; Table 1). The lithoclasts within the rock are similar in grain size to the crystalloclastic particles (Table 1). The particles are either cemented with calcite or supported by a dark matrix (Table 1).

5 Petrography and mineral chemistry of volcanoclastic rocks

Analysed rocks are composed of two-fold mineral associations. The first group of volcanoclastic rocks, related to *autoclastic effusive facies* and *resedimented autoclastic facies* largely consists of basaltic lithoclasts. There, plagioclase and pyroxene are the principal crystal phases (Fig. 3C, E, G). Alternatively, these phases may also be found as crystalloclasts (Fig. 3F). The rocks of the *secondary pyroclastic facies* are dominated by crystalloclasts of plagioclase

(Fig. 3I), K-feldspar and quartz (Fig. 3J). Their grain sizes are noticeably greater in the *coarse-sized ash crystalloclastic tuff* (Fig. 3I) compared to the *fine-sized ash crystalloclastic tuff* (Fig. 3J, K).

Phase chemistry of representative phases from basalt (clasts in *resedimented autoclastic facies*) is shown in Additional file 2: Table S1 and Additional file 3: Table S2. Analysed rocks consist of up to 1.5 mm in size idiomorphic to hypidiomorphic prismatic K-feldspar ($An_{1-3}Ab_{9-16}Or_{83-90}$; Fig. 4A) characterized by homogenous chemical composition. Plagioclase grains are idiomorphic to hypidiomorphic zonal and lamellar (An_{13-33} ; Fig. 4A). Homogenous subhedral pyroxene has diopside composition ($Wo_{47-48}En_{41-42}Fs_{11-11}$; Fig. 4B) with higher Al_2O_3 content (5.70–6.12 wt.%) and Cr_2O_3 (0.38–0.85 wt.%), and uniform Mg# (~79.50). Secondary amphibole occurs as alteration products and is very rare. It was classified as magnesiohornblenda to tremolite (Fig. 4C) with the Mg# ranging from 45.6 to 71.0. Numerous secondary phases found in the matrix, vesicles, pumice fragments, and in the hyaline clasts are very fine fan-like aggregates of chlorite-like phases (diabantite and pycnochlorite, Hey, 1954; Fig. 4D or Mg-chlorite (clinocllore), Zane & Weiss, 1998; Fig. 4E) and radial needle-like aggregates of Fe-pumpellyite (Fig. 4F) with low Mg# (18.2–38.6). Accessory minerals found sometimes as inclusions of plagioclase or in the fine volcanic matrix are apatite. Volcanic glass in the form of matrix in all determined facies has been altered to the assemblage of chlorite-like and to a lesser degree micaceous phases. X-ray diffraction analyses on a global sample from *secondary pyroclastic facies* (Additional file 1: Figure S1) revealed the dominance of chlorite-smectite (C-S), which is the typical high-temperature alteration product of igneous lithologies in the study area (Slovenec & Šegvić, 2021; Šegvić et al., 2023). The smectitization however has been attributed to the opening of 14 Å phyllosilicates during a low-temperature regime (Millot, 1971; Uzariwicz et al., 2012) ultimately leading to the formation of smectite-poor C-S of low periodicity and variable ordering (Additional file 1: Figure S1). Such defined composition of C-S aligns well with the microprobe data recording somewhat elevated content of alkali and earth-alkali elements (Additional file 3: Table S2). Comparatively less abundant alteration product is mica, likely a member of the illite–alumoceladonite series based on the position of its first basal reflex, presenting a final stage of the post-magmatic evolution of feldspar and glassy component (Slovenec et al., 2020).

6 Bulk-rock chemistry and Nd isotope composition of volcanoclastic rocks

The chemical composition of the representative rock samples is shown in Additional file 4: Table S3. Analysed samples belonging to the *autoclastic effusive facies* and *resedimented autoclastic facies* (Fig. 2) show identical chemical composition and will therefore be considered as a single chemical group in further discussion. Their silica content ($SiO_2=46.68–50.06$ wt.%) is characteristic for mafic igneous extrusive rocks (Cox et al., 1979, page 231). The exception is the analysed sample VU III-3 (Fig. 2) with the high silica content ($SiO_2=61.93$ wt.%). Based on the petrographic definition, this sample belongs to the *secondary pyroclastic facies* dominantly made of the felsic fine ash tuff. The trace element based classification diagram of Winchester & Floyd (1977) reveals the analysed rocks predominantly fall in the category of sub-alkali basalts. However, sample VU III-3 stands out as an exception due to its elevated Zr content, placing it within the rhyodacite field (Fig. 5A). The high values of Ce/Yb (>10) and Ta/Yb (>0.1) indicate their calc-alkaline affinity (Fig. 5B). Analysed volcanoclastics are characterized by moderately high TiO_2 content (up to 1.36 wt.%) and Al_2O_3 (up to 18.84 wt.%), and moderately low MgO content (up to 5.45 wt.%) with significant variations in CaO (2.15–12.71 wt.%). Some of the samples exhibit higher K_2O values (≤ 3.61 wt.%). The loss of ignition (LOI) is between 3.60 (rhyodacite tuff sample) and 8.09 wt.%, which points to the medium level of post-magmatic alterations (Polat et al., 2002; Polat & Hofmann, 2003). Since some elements may be mobile during deuteric alterations we tested the element mobility by plotting their concentrations against that of Zr (not shown). This approach showed variable and selective mobilization of some major elements (Ca, Na, K) and large ion lithophile elements (LILE) such as Cs, Rb, K and Ba. By contrast, high field strength elements (HFSE) like Th, Nb, Ta, Ti, Hf, P, Y, and rare earth elements (REE) remained largely immobile. They were therefore deemed suitable for petrogenetic considerations (Pearce & Norry, 1979; Shervais, 1982; Becaluva et al., 1983). The volcanoclastics show an evolved geochemical character and are moderately fractionated in terms of Mg#, Ni and Cr content (43.0–54.8, 8–25 and <57 ppm, respectively). Moderately high Zr content (103–166 ppm) in mafic volcanoclastics relates to the presence of zircon, which is abundantly documented in the rhyodacite tuff sample (Zr=372 ppm).

The N-MORB normalized incompatible element patterns are shown in Fig. 6A. All mafic rocks exhibit a wide range of LILE (Cs, Ba, Rb, K) and Th enrichment ranging from 3.2 to 500 times relative to N-MORB and nearly flat pattern for more immobile elements (Zr to Lu) which ranges from 0.8 to 2.4 times relative to N-MORB.

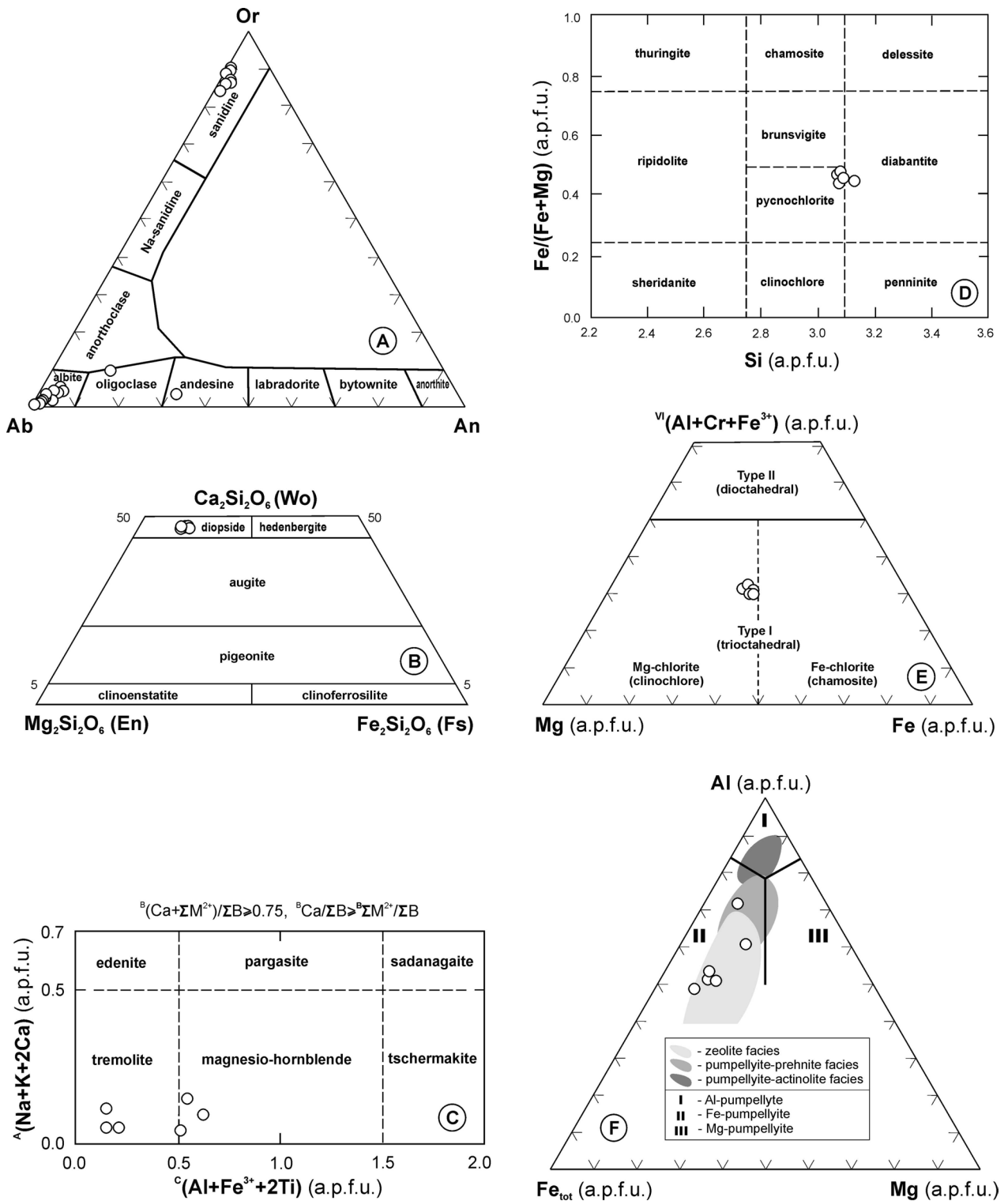


Fig. 4 Classification diagrams for **A** feldspar [Ab – An – Or plot; Deer et al., 1992, page 2; Dana et al., 1993, page 532], **B** pyroxene [En – Wo – Fs ($Mg_2Si_2O_6 - Ca_2Si_2O_6 - Fe_2Si_2O_6$) plot; Morimoto, 1988] **C** calcium amphibole [$^A(Na + K + 2Ca - ^C(Al + Fe^{3+} + 2Ti))$ plot; Hawthorne et al., 2012], **D–E** chlorite [Fe/(Fe + Mg) – Si plot (after Hey, 1954 adapted to Sun et al., 2019); Mg – Fe – $^V(Al + Cr + Fe^{3+})$ plot (Zane & Weiss, 1998)], **F** pumpellyite [$Fe_{tot} - Mg - Al$ plot (adapted after Passaglia & Gottardi, 1973; Coombs et al., 1976)] from the basaltic volcanoclastics from Mt. Ivanščica. The compositional fields of pumpellyite from the East Taiwan Ophiolite (zeolite facies), the Olympic Peninsula (prehnite–pumpellyite facies) and the Taveyannaz Formation (upper prehnite–pumpellyite and pumpellyite–actinolite facies) were taken from Mével (1981), Coombs et al. (1976) and Rahn et al. (1994)

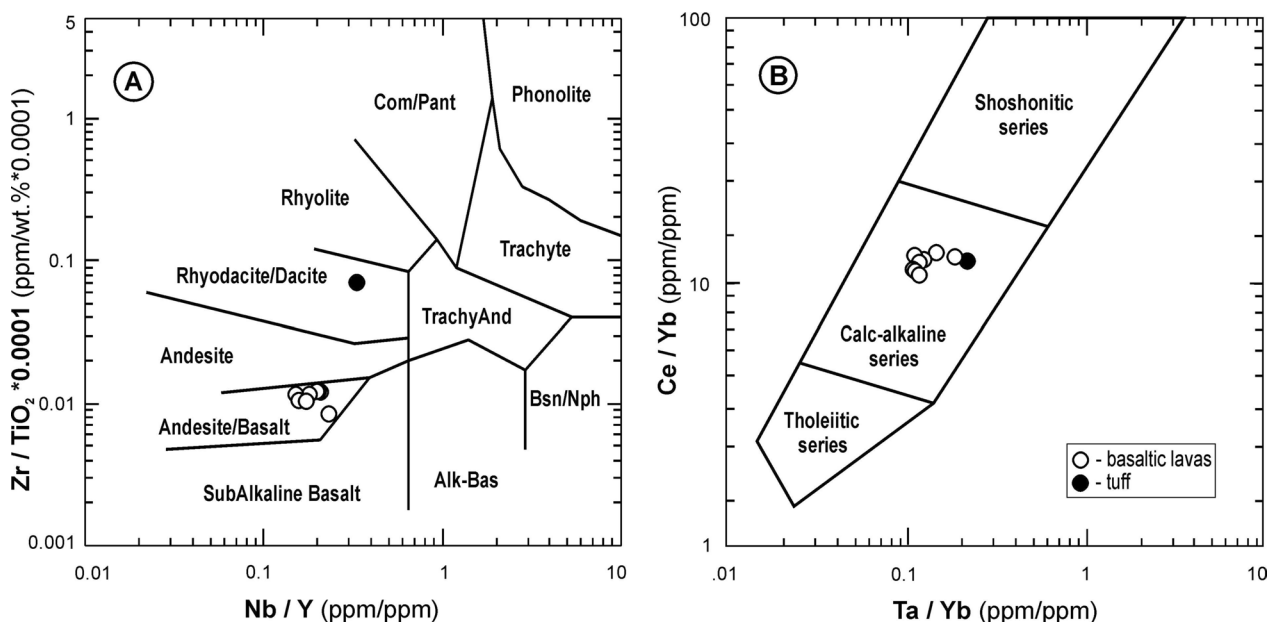


Fig. 5 **A** Nb/Y – Zr/TiO₂*10⁻⁴ classification diagram (Winchester & Floyd, 1977) and **B** Ce/Yb – Ta/Yb discrimination diagram after Pearce (1982) for the basaltic volcanoclastics and rhyodacite tuff from Mt. Ivanščica

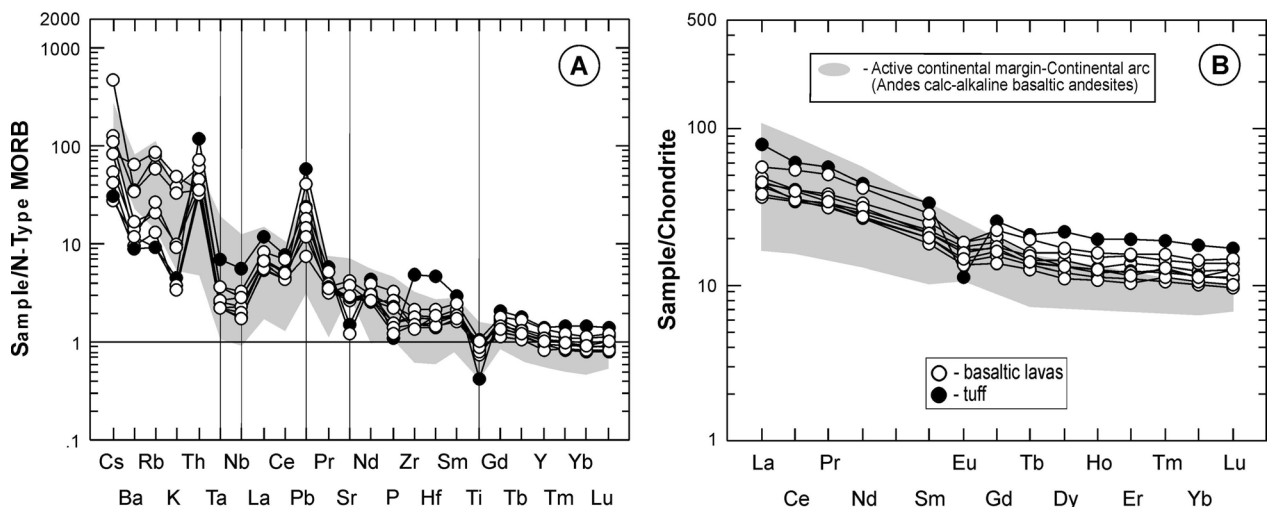


Fig. 6 **A** N-MORB-normalised multi-element and **B** REE patterns for the basaltic volcanoclastics and rhyodacite tuff from Mt. Ivanščica. Normalisation values are from Sun and McDonough (1989). Fields for Active continental margin-Continental arc calc-alkaline basaltic andesites in the Andes (Wilson, 1989, page 215) are plotted for comparison

A typical feature of all analysed samples is strong positive Pb spike [(Pb/Ce)_N = 1.67–9.14], as well as the significantly pronounced negative anomalies of the Nb–Ta pair [e.g., (Nb/La)_N = 0.30–0.48]. Further on, the documented negative anomalies of Sr and Ti are typical for the subduction-related magmas (Pearce et al., 1984; Hofmann, 1997). The intensity of the negative Ti anomaly and positive Pb anomaly is the highest in the rhyodacite tuff

sample (VU III-3). This most evolved felsic tuff is characterized also by a positive Zr-Hf anomaly which may suggest crustal contamination (Sun & McDonough, 1989) and zircon enrichment.

The chondrite normalized REE patterns are shown in Fig. 6B. Samples exhibit the same trend of their normalized concentrations which suggests an equal composition of fractionated phases. The highest normalized

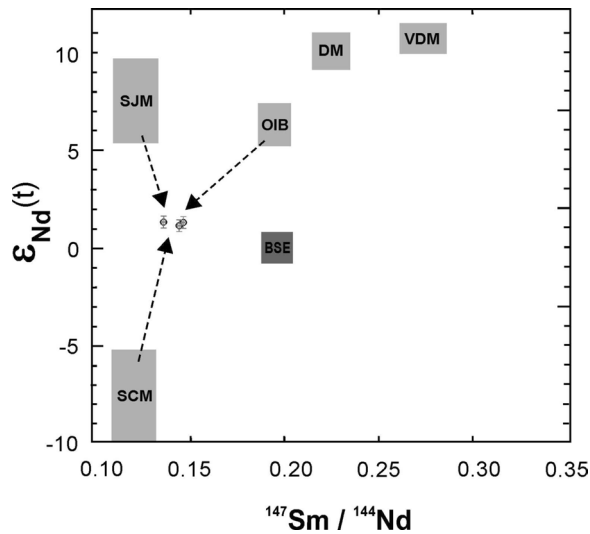


Fig. 7 $^{147}\text{Sm}/^{144}\text{Nd} - \epsilon_{\text{Nd}(t)}$ isotope ratios diagram for the basaltic volcanoclastics and rhyodacite tuff from Mt. Ivanščica. Hypothetical mantle sources: *DM* depleted mantle (not refractory), *VDM* very depleted mantle (refractory), *SJM* subducted juvenile material (subducted oceanic crust; slab with little pelagic sediment), *SCM* subducted continental material and *BE* bulk earth. The observed compositions and hypothetical end members sources calculated for the Middle Triassic following Swinden et al. (1990)

concentrations are documented in the rhyodacite tuff sample. The normalized REE patterns show enrichment of light rare earth elements (LREE) over heavy rare earth elements (HREE) $[(\text{La}/\text{Lu})_{\text{CN}} = 3.52\text{--}4.69]$ at 28–80 times chondrite relative concentrations. All samples show almost flat HREE profiles $[(\text{Tb}/\text{Lu})_{\text{CN}} = 1.14\text{--}1.40]$ at 10–21 times relative to chondrite. The slight negative Eu anomaly ($\text{Eu}/\text{Eu}^* = 0.74\text{--}0.88$) in analysed mafic volcanoclastics, is more pronounced in felsic pyroclastics ($\text{Eu}/$

$\text{Eu}^* = 0.38$) is typical for fractionation and removal of plagioclase in more evolved rock types (Sun & Nesbitt, 1978; Wilson et al., 1995).

The neodymium isotope composition of analysed rocks is provided in Additional file 5: Table S4. The values of $^{143}\text{Nd}/^{144}\text{Nd}$ of three representative samples are very consistent ranging from 0.512612 to 0.512622. The initial ϵ_{Nd} are calculated for 245 Ma which is the crystallization age of analysed basaltic lavas based on the Ar/Ar plagioclase dating (see below). The initial ϵ_{Nd} varies between $+1.22 (\pm 0.494)$ to $+1.35 (\pm 0.510)$. These low values above the bulk silicate earth suggest a moderate degree of crustal contamination. However, the complexity of the source areas and associated melts from which the investigated lavas were generated is indicated by the $\epsilon_{\text{Nd}(t)}$ vs. $^{147}\text{Sm}/^{144}\text{Nd}$ diagram at which points are plotted in the transition zone between OIB, SJM and SCM (Fig. 7).

7 $^{40}\text{Ar}/^{39}\text{Ar}$ dating

The results of $^{40}\text{Ar}/^{39}\text{Ar}$ dating on plagioclase separates from sample VU II-1 are provided in Additional file 6: Table S5, while the ^{39}Ar release spectra are shown in Fig. 8A. The calculations based on the released spectra indicated an age of 244.5 ± 2.8 Ma. This corresponds to the Middle Triassic (Anisian-early Ladinian, Gradstein et al., 2020). Sample VU II-1 is determined as *coarse-sized ash lithoclastic tuff* lithotype of the *resedimented autoclastic facies*.

Slovenec & Šegvić (2021) reported K–Ar ages of 241.1 ± 5.2 Ma for high-K calc-alkaline lavas and associated pyroclastic products on Kuna Gora Mt. in NW Croatia. Furthermore, the crystalloclastic and vitriclastic tuffs recovered from north-western Croatian mountains which were classified as deposits of a syn-eruptively resedimented *pyroclastic density flow*, are constrained

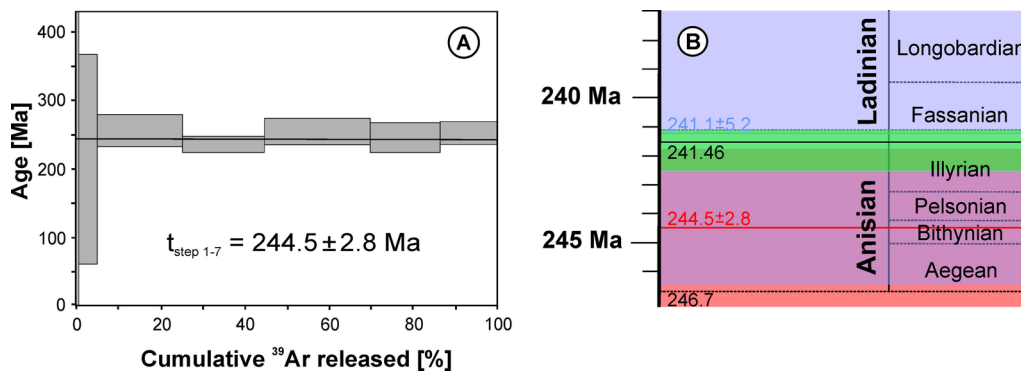


Fig. 8 **A** $^{40}\text{Ar}/^{39}\text{Ar}$ step heating diagram of *coarse-sized ash lithoclastic tuff* lithotype of the *resedimented autoclastic facies* (sample VU II-1) from Mt. Ivanščica. **B** Age constraints of the *coarse-sized ash lithoclastic tuff* lithotype of the *resedimented autoclastic facies* from the Vudelja quarry (transparent red) combined with the radiolarian ages of the felsic tuff deposits in the southern part of the Ivanščica Mt. (transparent green – Kukoč et al., 2023) and K–Ar ages obtained from high-K calc-alkaline lavas and associated pyroclastic products on Kuna Gora Mt. (transparent purple – Slovenec & Šegvić, 2021)

biostratigraphically to the late Illyrian-early Fassanian (Kukoč et al., 2023). *Secondary pyroclastic facies* deposits (sensu Di Capua et al., 2022) of felsic tuffs in the present study have similar characteristics as volcanogenic deposits recorded in Kukoč et al. (2023).

Ages reported by Slovenec and Šegvić (2021), Kukoč et al. (2023) and those from this study are shown in Fig. 8B.

8 Discussion

Three volcanoclastic facies have been recognized in the investigated outcrop: (I) *autoclastic effusive facies*, (II) *resedimented autoclastic facies* and (III) *secondary pyroclastic facies*. Their distribution in the abandoned quarry front is shown in Fig. 2. The spatial organization and distribution of determined facies are not clearly visible in the whole quarry front due to thick and abundant scree,

and tectonic disruptions. In today's configuration, the distance from the primary volcanic source area likely increased from north-west to south-east.

8.1 Genesis of volcanoclastic facies

Volcanoclastic facies can be categorized into two groups based on their geochemical composition (Table 1). The first group primarily consists of basaltic lavas which underwent autoclastic processes, followed by re-sedimentation and reworking. Tectonic activity related to the rifting of the future Neotethys Ocean caused severe faulting and formation of graben and half-graben structures (Fig. 9). Basaltic magma likely effused through these deep fractures in the oceanic crust in the form of fissure-like effusions (Fig. 9). Such basalts are shown in Fig. 9 as basalt effusions of the *coherent facies* (CF). Primary basaltic effusions of the *coherent facies* were not recorded in the Vudelja quarry. The *autoclastic effusive facies* (AF)

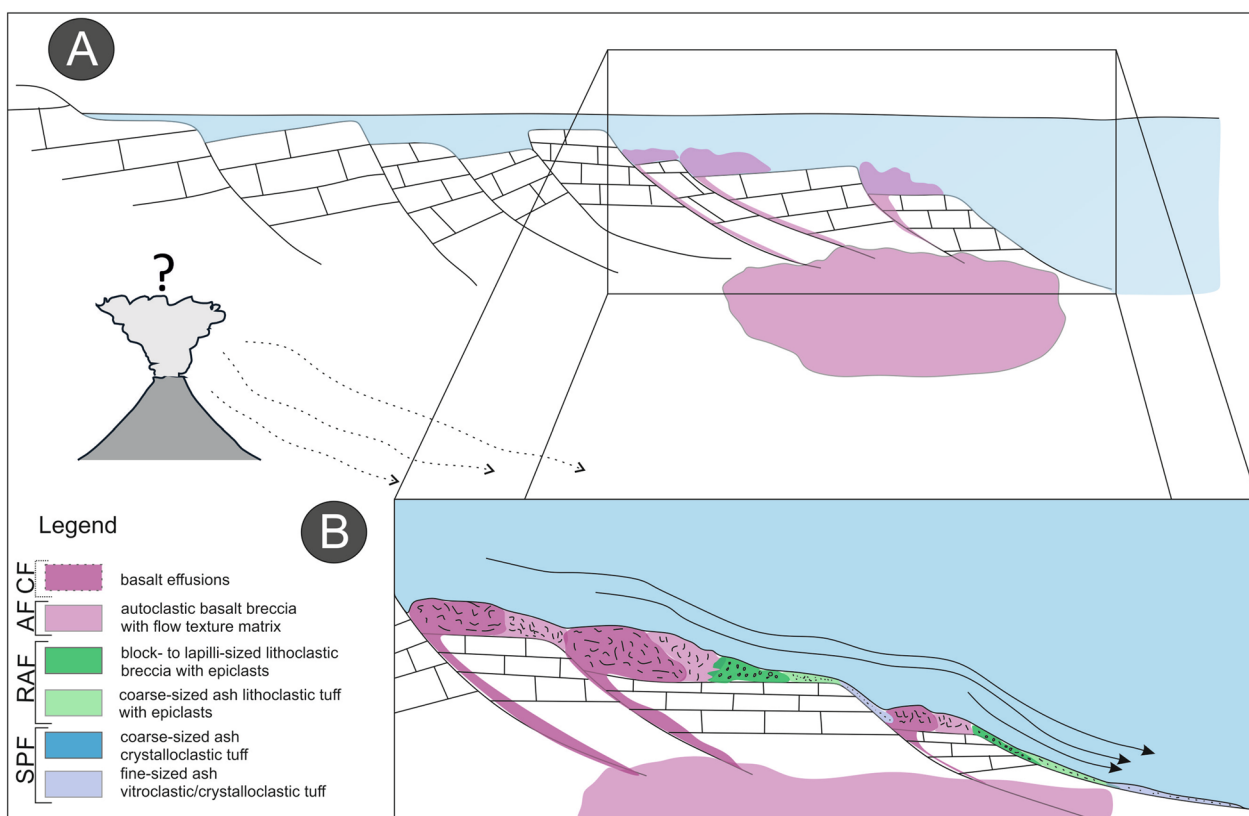


Fig. 9 Volcano-sedimentary model representing mechanisms of formation and spatial distribution of generated facies during their time of formation. **A** A wider image representing the horst-graben, half-graben structure that was created by normal faulting related to the Middle Triassic rifting. These fault fractures served as routes for basaltic magma ascent and effusions. **B** The effused basaltic magma is quenching and autofragmenting in contact with cold sea water. Since slopes were developed during the faulting, newly formed basaltic clasts are transported by gravity currents. The most proximal clastic material is still influenced by effused lava, while with the alienation from the source the fragments become finer and are supported by sedimentary type matrix or cemented by calcite cement precipitated from the sea water. The *secondary pyroclastic facies* are deposited here as syn-eruptively resedimented PDC deposits from the explosive eruptions from an unknown/undiscovered source

and *resedimented autoclastic facies* (RAF) are genetically linked and their distribution indicates an increasing distance from the original volcanic source (CF) and more pronounced re-sedimentation processes occurring further away. *Autoclastic effusive facies* deposits formed as a result of material fragmentation due to the rapid cooling of lava entering the marine environment. Clasts formed by these processes are irregular in shape and poorly sorted (Table 1). Different textures of basaltic clasts indicate that different parts of the flow were fragmented. It is however possible that some of the clasts stemming from hypothetical previous effusions might have been incorporated into the deposits of the *autoclastic facies* during transport. The newly formed clasts are subsequently redeposited by gravitational mechanisms (McPhie et al., 1993). The occurrence of a hyaline matrix with a flow texture documented in the samples of *autoclastic effusive facies* (Table 1; Fig. 3C) suggests relatively short sediment transport and permeation of the glassy lava flow in between the newly formed clasts (Allen, 1988).

Carbonate clasts found within volcanoclastic deposits (Fig. 3A) originated from the shallow marine carbonate environment (Table 1; Fig. 3B). Intense tectonic movements likely led to the coeval existence of active carbonate platform(s) and deeper marine environments (Goričan et al., 2005; Kukoč et al., 2023). The epiclasts of pelagic limestones (micritic limestone with pelagic fossils) found in both facies (AF and RAF) could have been incorporated in the volcanoclastics as they were moving over the carbonate bedrock, or/and due to the ascent of magma which had fragmented the bedrock. Pelagic limestone was deposited on subsided blocks within the NCTRB during the Middle Triassic (Kukoč et al., 2023). Carbonate clasts do not exhibit features that would suggest direct contact with hot volcanic rocks.

With the more distal transport from the primary basaltic magma effusion, clasts become rounder due to reworking (Table 1). The consistent composition of basaltic clasts suggests that there has been no alteration in the source area (Table 1; Fig. 9). The primary distinction between the *autoclastic effusive facies* and the *resedimented autoclastic facies* can be seen as the absence of a flow-type hyaline matrix between the clasts of the latter. The *resedimented autoclastic facies* is characterized by a prevalent sedimentary type of matrix, consisting of fine particles (Table 1). In places, clasts may have been cemented by calcite. The absence of hyaline lava in this facies implies that the lithotypes were deposited at greater distances from the source, where hyaline lava could have not penetrated the deposits. Rare occurrences of lithoclasts of vitroclastic tuffs indicate erosion of *secondary pyroclastic facies* which likely existed somewhere laterally. Both lithotypes of RAF, namely *lapilli-sized*

basalt breccia with epiclasts and *coarse-sized ash lithoclastic tuff with epiclasts*, are found near each other at the quarry front (Fig. 2). The variations in clast size can be attributed to the sorting which occurred during transport and deposition. The material for this facies was likely transported downslope from submarine heights and deposited in deeper parts of the depositional environment by gravitational currents (Fig. 9). The grading texture visible in some samples (Table 1; Fig. 3H) supports this interpretation. In general, sedimentary processes had a stronger influence over the volcanic activity in shaping this facies.

The second geochemical group of facies is presented by *secondary pyroclastic facies* (SPF) (sensu Di Capua et al., 2022). The *coarse-sized ash crystalloclastic tuff* lithotype is determined as a single narrow zone (Fig. 2). Although there is no available chemical analysis for this specific sample, the phase assemblage indicates a felsic to intermediate composition (Table 1). The prominent feature of this sample is the pronounced imbrication of existing crystalloclasts and elongated pumice fragments, which signifies the processes of deposition by traction currents (Table 1, Fig. 3I). The plastic deformation observed in pumice fragments in contact with crystalloclasts indicates that the pumice fragments remained ductile while the current was in motion, indicating their syn-eruptive redeposition. Basaltic lithoclasts could have been incorporated while the current was moving over the basalts and/or basaltic volcanoclastics.

Fine-sized ash vitroclastic and *crystalloclastic tuffs* of the *secondary pyroclastic facies* are geochemically determined as rhyodacite tuff (Fig. 5A). The main characteristic of these deposits is the dominance of horizontal to wavy lamination (Table 1). The presence of lamination is attributed to the transition from predominantly crystalloclastic particles to vitroclastic particles. Similar associations of lithotypes has been reported in other locations within the NCTRB. They are determined as deposits of the distal *pyroclastic density flows* generated by volcanic eruptions from vents located near the shore and syn-eruptively redeposited by turbidite-like currents. These lithologies are widely recognized in the neighboring region of the Alpine-Dinaridic belt and are commonly referred to as *Pietra Verde tuffs* (e.g. Castellarin et al., 1988, Oberholzner, 1991). Storck et al. (2020) indicated several (sub-) volcanic centers in the Alpine region, that were active from 241.913 ± 0.052 to 238.051 ± 0.053 Ma, as a possible source of this pyroclastic material. Such volcanic centres have not been described from the Dinaridic region, except for a relatively small dolerite body (Slovenec et al., 2023a), indicating that the same Alpine explosive (sub-) volcanic centres could have served as a source of pyroclastic material for the wider region of the

Greater Adria. An alternative explanation for the absence of such a volcano in the Dinarides could be attributed to its presumed proximity to the ancient shoreline or potentially even its location within shallow-water environment. In that case, seawater could be incorporated into the volcanic vent system producing vapour and raising the pressure in the magma chamber, thus causing explosive eruptions able to produce a huge amount of pyroclastic material. In addition, the energy of waves could have reworked a vast majority of that volcanic/volcanoclastic material. These processes could have produced material for secondary volcanogenic detritus found in younger deposits, such as the Wengen Formation in the Alpine region (Brack & Rieber, 1993; Gianolla et al., 1998; Brack et al., 2005; 2007) or the secondary volcanoclastic deposits of the NCTRB (Kukoč et al., 2023). The deposition of fine ash PDC material most likely occurred during the waning phase of volcanic activity that produced the basaltic lavas, along with the redeposition of basaltic clasts. A similar scenario has been documented in the current Ethiopian rift system today (Kazim et al., 1980; Wolde Gabriel & Aronson, 1987; Wolde Gabriel et al., 1990; Bonini et al., 2005). There, the presence of basalts along with intermediate and felsic rocks has been documented and interpreted this as evidence of bimodal volcanism occurring in the Eastern Africa rift area (Morbidelli et al., 1975; Zanettin et al., 1978; Wolde Gabriel et al., 1990; Mazzarini et al., 1999; Bonini et al., 2005). Analogous situations of both modern and ancient volcanic systems are described by Ellis and King (1991), Jackson et al. (2008), and Hnylko et al. (2015).

Felsic tuffs of NW Croatia intercalated with radiolarian cherts were dated as late Illyrian to early Fassanian (Goričan et al., 2005; Slovenec et al., 2023b; Kukoč et al., 2023). Basaltic volcanoclastics were dated radiometrically at 241.1 ± 5.2 Ma (Slovenec & Šegvić, 2021). Therefore, in the case of Middle Triassic deposits of NW Croatia the existence of andesitic to basaltic volcanic/volcanoclastic rocks (Slovenec & Šegvić, 2021; Slovenec et al., 2020; Kukoč et al., 2023), as well as rhyolitic to rhyodacitic coarse to fine ash tuffs (Goričan et al., 2005; Slovenec et al., 2023b; Kukoč et al., 2023) indicates a bimodal volcanic activity in the region of the Greater Adria during the Middle Triassic (Fig. 6).

In the wider Dinaridic region, traces of Middle Triassic volcanic activity are recorded in a variety of settings. Although it is speculated that the initial volcanic activity started in the Permian (Šćavničar, 1979) and lasted up to the Late Triassic (Pamić, 1984), the peak of the volcanic activity in the Dinarides occurred during the Middle Triassic. The remnants of this volcanic activity are observed through the presence of basaltic and andesite sub-/effusions (Pamić, 1984; Lugović & Majer, 1983;

Dimitrijević, 1997; Trubelja et al., 2004; Slovenec et al., 2023a), more evolved effusive rocks (Dimitrijević, 1997), intrusive igneous rocks (Golub & Vragović, 1975; Marić, 1976; Pamić, 1984, 2000; Trubelja et al., 2004), and volcanoclastic deposits (Šćavničar et al., 1984; Marci et al., 1991; Belak, 2000; Kolar-Jurkovšek et al., 2006; Balini et al., 2006; Aljinović et al., 2010; Gawlick et al., 2012; Smirčić et al., 2018, 2020a; 2020b). The majority of volcano-sedimentary successions, which have been dated using biostratigraphic or isotopic methods, indicate a late Illyrian to early Fassanian age (e.g., Gawlick et al., 2012; Smirčić et al., 2018, 2020b). Mafic volcanoclastic deposits, similar to the ones recorded in this study and interpreted as submarine effusions, are found in the External Dinarides (Šćavničar et al., 1984; Smirčić et al., 2018). Here, mafic volcanoclastics have been accompanied by felsic *Pietra Verde*-type tuffs (Šćavničar et al., 1984), and covered by shallow-water carbonates. *Pietra Verde*-type tuffs in the successions of the External Dinarides, exhibit characteristics of gravitationally-driven submarine deposits as well. Here, the effusive volcanism seems to have ceased in the early Carnian (Pamić, 1984; De Min et al., 2008).

Volcanic and volcanoclastic deposits are a common feature of Middle Triassic deposits of the Southern Alps and the Transdanubian Range. Mafic volcanic and volcanoclastic deposits, including pillow lavas and hyaloclastites were deposited in a deep-marine environment (Bosellini et al., 2003) in the Alpine region. These deposits have been referred to as the Fernazza Formation (Mundil et al., 1996; Brandner et al., 2007) and are dated as 238.65 Ma to 237.77 Ma, which corresponds to the late Ladinian (Gradstein et al., 2020). *Pietra Verde* tuffs are intercalated within the coeval basinal and shallow-water deposits and have been constrained radiometrically from 242.65 Ma (late Illyrian) to 237.58 Ma (late Ladinian to early Carnian) according to Storck et al. (2018). These obtained age span suggests a coeval existence of the two different types of volcanism analogue to the study area of the NCTRB. However, while the ages of felsic volcanic products are comparable, mafic volcanites and volcanoclastics of the Fernazza Formation are somewhat younger than the mafic lithologies in the NCTRB. Lithologies similar to the ones presented in this study have also been documented in Transdanubia and Gemer-Bükk subunits of the Alcapa Block (Harangi et al., 1996; Velledits, 2004, 2006). In the Transdanubian Range, Middle Triassic volcanic and volcanoclastic lithologies, along with pyroclastic deposits, are present in two distinct horizons: one ranging from the Anisian to the early Ladinian, and the other occurring in the late Ladinian. The main difference between the two relates to their chemical composition. The older horizon is composed of intermediate to felsic

volcanic lithologies, while the younger belongs to the alkaline basaltic series (Harangi et al., 1996).

Based on the available data, it can be tentatively concluded that the mafic effusion in NW Croatia occurred earlier than in the Southern Alps and Transdanubian Range. This observation suggests that the present-day Dinarides were positioned closer to the main rifting direction of the future Neotethyan Ocean (Fig. 46 in van Hinsbergen et al., 2020; or Fig. 12 in Slovenec et al., 2023a, 2023b). The *Pietra Verde* tuffs are found throughout the entire area as extensive horizons, ranging in age from the late Illyrian to late Ladinian. Similar to the Southern Alps and the Dinarides, this indicates that such pyroclastic activity persisted concurrently with the mafic effusions during that period.

8.2 Petrogenesis of parental lavas

The complex origin of analysed rocks from all three determined facies in the Vudelja Quarry can be clarified based on the ratios of discriminant trace elements and the Sm–Nd isotope data. Low and constant Sm/La coupled with a moderately high Th/La ratio (up to 0.52; Fig. 10) indicate the presence of sediment/crustal material in the generation of the magmas. Positive Pb spikes (up to 12.2; Fig. 6A) clearly reveal elevated degrees of crustal contamination. Low positive values of initial $\epsilon_{Nd(t)}$ (≤ 1.34) and low values of $^{147}\text{Sm}/^{144}\text{Nd}$ (≤ 0.137401 ; Additional file 5: Table S4) coupled with negative anomalies of Nb–Ta pair relative to

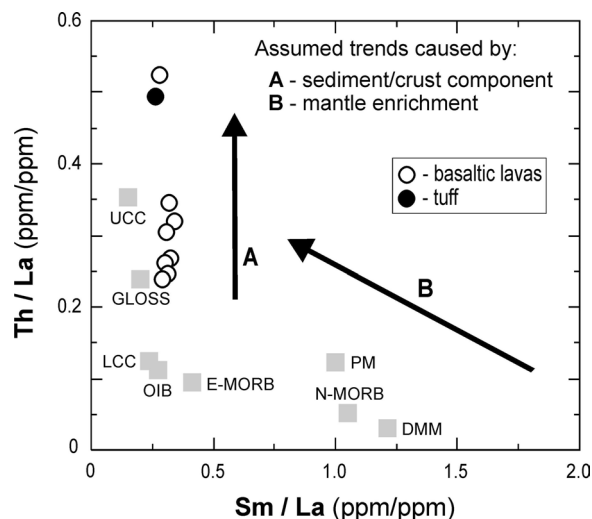


Fig. 10 Discrimination diagrams for the basaltic volcanics and rhyodacite tuff from Mt. Ivanščica. Th/La – Sm/La (after Plank, 2005). *N-MORB* normal mid-ocean ridge basalts, *E-MORB* enriched MORB, *OIB* ocean island basalts, *PM* primitive mantle (Sun & McDonough, 1989); [*UCC* upper continental crust, *LCC* lower continental crust (Taylor & McLennan, 1985); *GLOSS* global subduction sediment (Plank & Langmuir, 1998); *DMM* depleted MORB mantle (Workman & Hart, 2005)

La (Fig. 6A) are in line with the input of subducted slab melts. The magma responsible for the formation of the investigated rocks was generated through partial melting, which occurred as a result of the mixing of three distinct source components: (a) subducted juvenile material (SJM) whose origin was likely linked to the subducted oceanic crust of the Paleotethys, (b) subducted continental material (SCM), i.e. sediments recycled in mantle wedge and (c) subordinate of OIB-like mantle (Fig. 7).

The petrogenetic model based on incompatible and immobile trace element concentrations (i.e. Dy vs. Yb, Rollinson, 1993, page 166; Thirwall et al., 1994) was used to report on partial melting of a residual mantle source. In the Dy/Yb vs. Yb diagram (Fig. 11) analysed basaltic rocks plot near the melting curve representing a spinel mantle source region, and the partial melting degree could have spanned from 7 to 13%. This generally low degree of spinel source partial melting reflects a relatively shallow mantle source probably related to a mature volcanic arc.

In brief, it can be inferred that the analysed calc-alkaline rocks from all three facies were formed as a result of complex processes involving partial melting of the metasomatized subcontinental lithospheric mantle, along with minor melting of a shallow asthenospheric mantle.

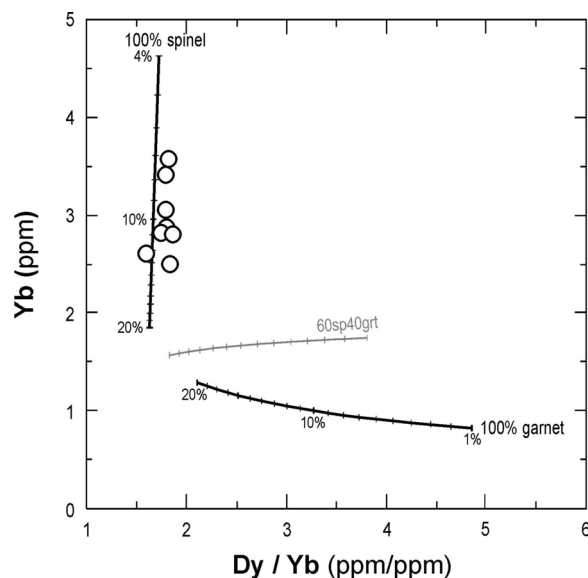


Fig. 11 Yb – Dy/Yb diagram for the basaltic volcanics from Mt. Ivanščica. Partial melting curves are shown for the non-modal batch melting of spinel and garnet-herzolite sources, starting from a Primitive Mantle (PM; McDonough & Frey, 1989) material. Mineral and melt modes for spinel and garnet-herzolite source: $\text{Ol}_{0.58(0.10)} + \text{Opx}_{0.27(0.27)} + \text{Cpx}_{0.12(0.50)} + \text{Sp}_{0.03(0.13)}$ (Kinzler, 1997) and $\text{Ol}_{0.60(0.05)} + \text{Opx}_{0.21(0.20)} + \text{Cpx}_{0.08(0.30)} + \text{Gt}_{0.12(0.45)}$ (Walter, 1998), respectively. Italic numbers in parentheses indicate the percentages of each mineral entering the liquid. Partition coefficients are from McKenzie & O'Nions (1991)

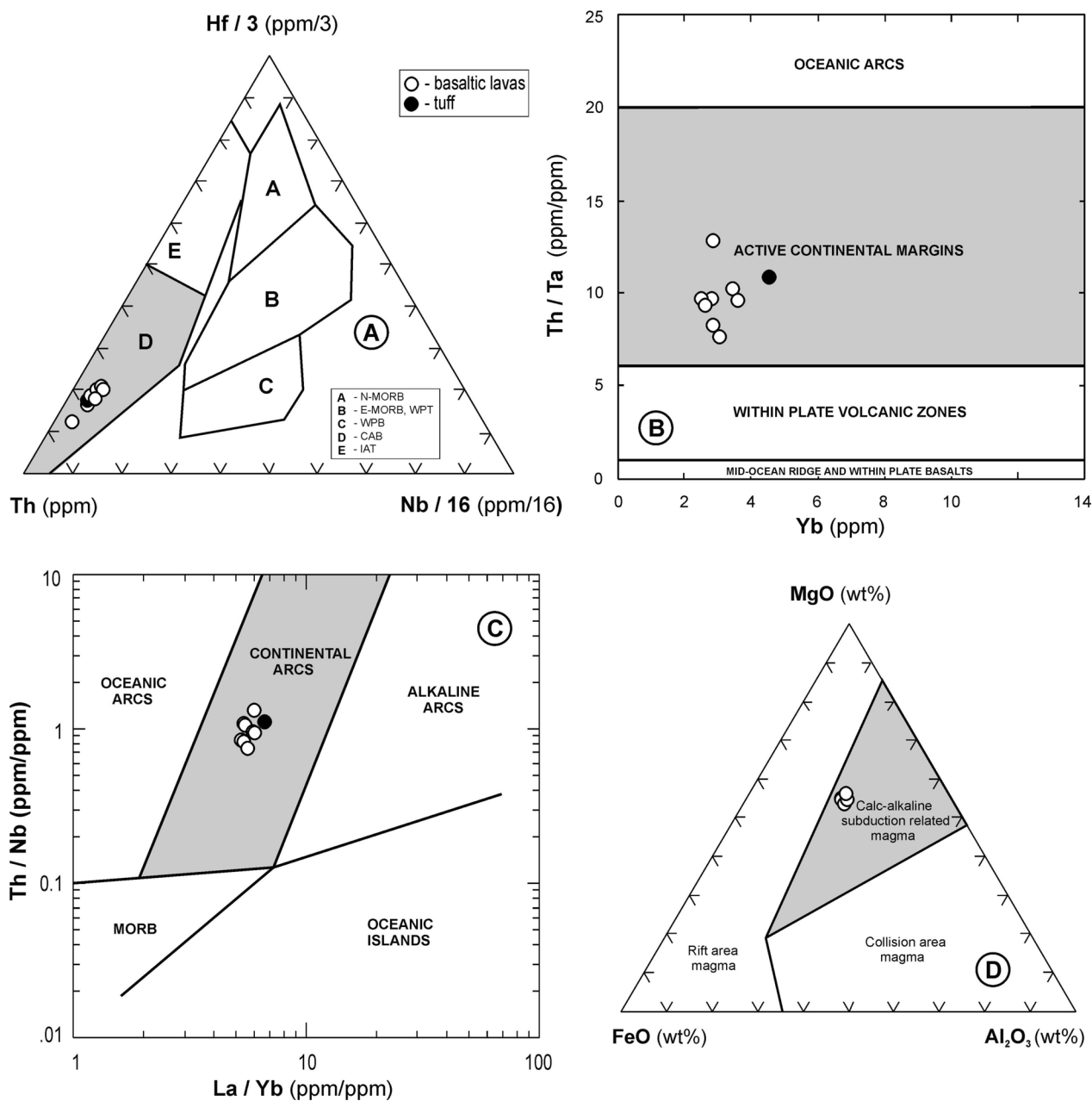


Fig. 12 Discrimination diagrams for the basaltic volcanoclastics and rhyodacite tuff from Mt. Ivanščica. **A** Th – Nb/16 – Hf/3 diagram (Wood, 1980). A = normal mid-ocean ridge basalts (N-MORB); B = enriched MORB (E-MORB) and within-plate tholeiites (WPT); C = alkaline within-plate basalts (AWPB); D = calc-alkali basalts (CAB); E = island-arc tholeiites (IAT). **B** Yb – Th/Ta diagram for felsic and intermediate rocks (Gorton & Schandl, 2000). **C** La/Yb – Th/Nb diagram (Hollocher et al., 2012). **D** FeO – Al₂O₃ – MgO discriminant diagram for pyroxene (Le Bas, 1962)

8.3 Tectonomagmatic and geodynamic significance

Analysed basaltic volcanoclastic rocks and associated rhyodacitic tuffs from the Vudelja Quarry exhibit chemical characteristics of calc-alkaline magmas formed in the volcanic arc geotectonic settings, which suggests a genetic relation with the subduction zone (Fig. 12A-C). The chemical composition of the primary mineral phases

further supports the same conclusion (clinopyroxene; Fig. 12D). Enrichment in LILE and LREE concentrations and negative anomalies of Nb–Ta and Ti (Fig. 6A, B), along with depletion in HFSE and Th/Ta vs. Yb and Th/Nb vs. La/Yb ratios (Fig. 12B-C) support a strong subduction influence (e.g. Pearce, 1982, 1983; Arculus & Powel, 1986; Hawkesworth et al., 1993, 1997). These findings

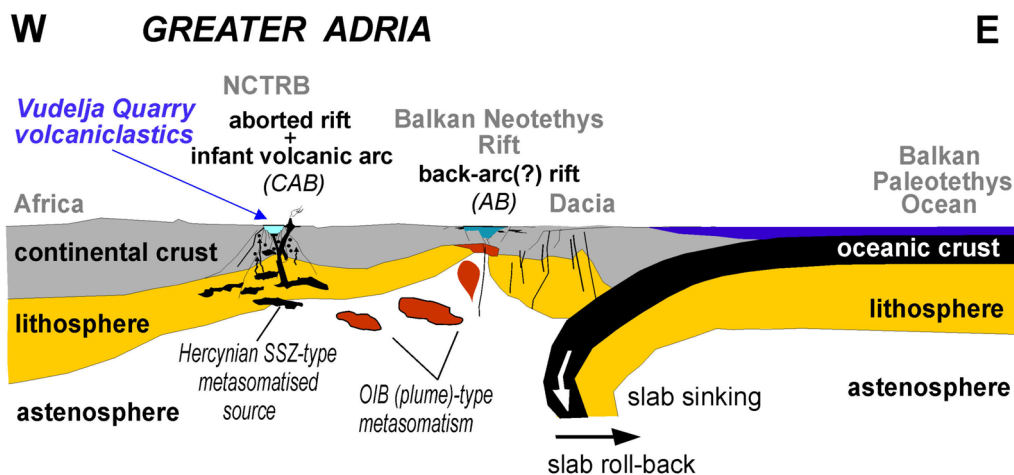
are consistent with the origin of the investigated volcanoclastic rocks being related to an ensialic and mature volcanic arc setting that developed in an active, Andean-type, continental margin environment. Nevertheless, the observed chemical composition, indicating the presence of an active volcanic arc, is likely predominantly inherited from older arc-related lithologies associated with the subduction of the Paleotethys Ocean. As a result, it may not accurately reflect the true tectonomagmatic setting of the formation of the investigated volcanoclastic rocks and related basaltic lavas that served as their primary source. Their origin can be explained by the model of a passive continental rifting along mid-Triassic margins of the Greater Adria within the NCTRB (Fig. 13). This model includes (i) partial melting of the heterogeneous lithospheric (subcontinental) mantle, which had been metasomatized during an earlier Hercynian subduction event(s) in the Late Paleozoic (Saccani et al., 2015) and (ii) significantly subordinated to the processes related to the melting of the upper continental crust and fractionation as suggested by Slovenec & Šegvić (2021) for the coeval basalts/andesites of the wider study area.

9 Conclusions

Three different volcanoclastic facies are determined in the study area based on their micropetrographical characteristics: (I) *autoclastic effusive facies*, (II) *resedimented autoclastic facies*, and (III) *secondary pyroclastic facies*. These facies are divided into mafic and intermediate/felsic

groups based on geochemical results. The mafic group of facies: *autoclastic effusive facies* and *resedimented autoclastic facies* is composed dominantly of basaltic clasts with grain size change reflecting the increasing distance from the primary basaltic effusion. These facies were generated through basaltic fissure eruptions in a marine environment, where they underwent processes such as quenching, autofragmentation, and resedimentation of the freshly derived basaltic clasts. Additionally, the presence of limestone epiclasts containing distinct Middle Triassic reef fauna suggests the existence of a nearby shallow carbonate environment from which the carbonate fragments could have been sourced. The intermediate/felsic facies is determined as *secondary pyroclastic facies*. The secondary pyroclastic facies is characterized by the presence of horizontal lamination in fine ash tuffs (*Pietra Verde*), indicating distal parts of PDC deposits and their syn-eruptive redeposition. The geochemical characteristics of rocks from all analysed facies indicate a unique, relatively shallow, spinel mantle magma source. The magma was generated through a complex process involving the mixing of three distinct source components: (a) subducted juvenile material (SJM) whose origin was likely linked to the subducted oceanic crust of the Paleotethys Ocean, (b) subducted continental material (SCM), i.e. sediments recycled in the mantle wedge and (c) an OIB-like mantle.

The Ar/Ar dating revealed the ages of 244.5 ± 2.8 Ma, corresponding to the uppermost Spathian to uppermost Illyrian. This age coincides with the ages obtained for



Middle Triassic (Late Anisian-Early Ladinian)

Fig. 13 Schematic geodynamic model (scale is approximate) for ensialic infant arc – back-arc rifting in the central part of the Mediterranean region according to van Hinsbergen et al. (2020) palaeogeographic reconstruction. CAB calc-alkaline and shoshonitic basalts/volcaniclastites, AB alkaline basalts, OIB ocean island basalts, NCTRB Northwestern Croatian Triassic Rift Basin

felsic tuffs documented in the NCTRB, as well as in the wider area of the Greater Adria, suggesting that during the Middle Triassic time, the entire area of the Greater Adria was influenced by contemporaneous bimodal volcanism.

Supplementary Information

The online version contains supplementary material available at <https://doi.org/10.1186/s00015-024-00453-8>.

Additional file 1: Figure F1. X-ray diffraction analyses on a bulk sample of the secondary pyroclastic facies. Results suggest dominance of the chlorite-smectite minerals in the volcanic glass phase.

Additional file 2: Table S1. Representative chemical compositions and calculated mineral formulae of alkali-feldspar, plagioclase and clinopyroxene from the basaltic lavas from the Mt. Ivanščica.

Additional file 3: Table S2. Representative chemical compositions and calculated mineral formulae of amphibole, spinel, chlorite and pumpellyite from the basaltic lavas from the Mt. Ivanščica.

Additional file 4: Table S3. Chemical compositions of basaltic lavas/pyroclastics and rhyodacite tuff from the Mt. Ivanščica.

Additional file 5: Table S4. Nd isotope data of of basaltic lavas/pyroclastics from the Mt. Ivanščica.

Additional file 6: Table S5. $^{40}\text{Ar}/^{39}\text{Ar}$ data of plagioclase from basaltic lava (sample Vu II-1) from the Mt. Ivanščica.

Acknowledgements

This work has been supported by the Croatian Science Foundation under the project (IP-2019-04-3824). Florence Bégué and Luca Caricchi from the University of Geneva are thanked for providing excellent electron microprobe measuring conditions. The authors extend their gratitude to Branko Kordić and Josip Barbača from the Croatian Geological Survey for the drone imaging of the Vudelja Quarry. The authors would like to thank Špela Goričan and Emilio Saccani for their critical comments and constructive reviews, as well as the editorial handling by Daniel Marty and Boštjan Rožič that contributed significantly to the quality of paper.

Author contributions

DS: conceptualization, formal analysis, investigation, writing – original draft, visualization. MV: conceptualization, formal analysis, investigation, writing – original draft, visualization. DaS: conceptualization, formal analysis, investigation, writing – original draft, visualization, supervision, funding acquisition. DK: formal analysis, investigation, writing – review & editing, visualization. BŠ: formal analysis, investigation, resources, data curation, writing – review & editing. MH: formal analysis, investigation, writing – review & editing. MB: formal analysis, investigation, writing – review & editing. TG: formal analysis, investigation, writing – review & editing. LB: formal analysis, investigation.

Funding

This work has been supported by the Croatian Science Foundation under the project (IP-2019-04-3824).

Availability of data and materials

All data generated or analysed during this study are included in this article.

Declarations

Ethics approval and consent to participate

Not applicable.

Consent for publication

All authors have given their consent for publication.

Competing interests

The authors declare no competing interests.

Author details

¹Faculty of Mining, Geology and Petroleum Engineering, University of Zagreb, Pierottijeva 6, hr-10000 Zagreb, Croatia. ²Croatian Geological Survey, Ulica Milana Sachsa 2, 10000 Zagreb, Croatia. ³Department of Geosciences, Texas Tech University, 1200 Memorial Circle, Lubbock, TX 79409, USA. ⁴Covia Corporation, 4000 Baker Rd, Ottawa, IL 61350, USA.

Received: 31 October 2023 Accepted: 23 January 2024

Published online: 04 April 2024

References

- Aljinović, D., Kolar-Jurkovšek, T., Jurkovšek, B., & Hrvatović, H. (2010). Characteristics of some Middle Triassic volcanoclastic rocks in the External Dinarides (Croatia and Bosnia and Herzegovina). In: Horvat, M. (Eds). Abstract Book. 4th Croatian Geological Congress, Šibenik, Croatian Geological Survey, pp. 14–15.
- Allen, J. R. L. (1988). False pyroclastic texture in altered silicic lavas, with implications for volcanic-associated mineralization. *Economic Geology*, 83, 1424–1446.
- Arculus, R. J., & Powell, R. (1986). Source component mixing in the regions of arc magma generation. *Journal of Geophysical Research*, 91, 5913–5926.
- Babić, L. J. (1974). Jurassic-Cretaceous sequence of the Mt. Ivanščica (Northern Croatia). *Bull Sci Cons Acad Yugosl (A)*, 19(78), 181–182.
- Balini, M., Jurkovšek, B., & Kolar-Jurkovšek, T. (2006). New Ladinian ammonoids from Mt. Svilaja (External Dinarides, Croatia). *Rivista Italiana Di Paleontologia e Stratigrafia*, 12, 383–395.
- Bébién, J., Blanchet, R., Cadet, J. P., Charvet, J., Chorowitz, J., Lapiere, H., & Rampoux, J. P. (1978). Le volcanisme triasique des Dinarides en Yougoslavie: Sa place dans l'évolution géotectonique péri-méditerranéenne. *Tectonophysics*, 47, 159–176.
- Beccaluva, L., Di Girolamo, P., Macciotta, G., & Morra, V. (1983). Magma affinities and fractionation trends in ophiolites. *Ofoliti*, 8, 307–324.
- Belak, M. (2000). Postaja 2: profil Sutina-Zelovo Sutinsko; Kristaloklastični i vitroklastični tufovi (pietra verde) s proslojcima silicificiranih dolomita, vapnenaca, tufta i rožnjaka. In: Jelaska, V., Benček, Đ., Matičec, D., Belak, M., & Gušić, I. (Eds.). *Geološka povijest i strukturna evolucija Vanjskih Dinarida – Vodič ekskurzija* (Vlahović, I., Biondić, R., Eds.) 2. hrvatski geološki kongres, Cavtat-Dubrovnik, IGI, Zagreb, pp. 6–9.
- Bianchini, G., Natali, C., Shibata, T., & Yoshikawa, M. (2018). Basic dykes crosscutting the crystalline basement of Valsugana (Italy): New evidence of Early Triassic volcanism in the Southern Alps. *Tectonics*, 37, 2080–2093.
- Bonadiman, C., Coltorti, M., & Siena, F. (1994). Petrogenesis and T-fO₂ estimates of Mt. Monzoni complex (Central Dolomites, Southern Alps): A Triassic shoshonitic intrusion in a transcurrent geodynamic setting. *European Journal of Mineralogy*, 6, 943–966.
- Bonini, M., Corti, G., Innocenti, F., Manetti, P., Mazzarini, F., Abebe, T., & Pecskay, Z. (2005). Evolution of the main Ethiopian Rift in the frame of Afar and Kenya rifts propagation. *Tectonics*, 24(1), 1007.
- Bortolotti, V., Chiari, M., Marroni, M., Pandolfi, L., Principi, G., & Saccani, E. (2013). Geodynamic evolution of the ophiolites from Albania and Greece (Dinaric-Hellenic belt): One, two or more oceanic basins? *International Journal of Earth Sciences*, 102(3), 738–811.
- Bosellini, A., Gianolla, P., & Stefani, M. (2003). Geology of the Dolomites. *Epi-sodes*, 26, 181–185.
- Brack, P., & Rieber, H. (1993). Towards a better definition of the Anisian/Ladinian boundary: New biostratigraphic data and correlations of boundary sections from the Southern Alps. *Eclogae Geologicae Helvetiae*, 86, 415–527.
- Brack, P., Rieber, H., Mundil, R., Blendinger, W., & Maurer, F. (2007). Geometry and chronology of growth and drowning of Middle Triassic carbonate platforms (Cerner and Bivera/Clapsavon) in Southern Alps (northern Italy). *Swiss Journal of Geosciences*, 100, 327–348.
- Brack, P., Rieber, H., Nicora, A., & Mundil, R. (2005). The global boundary stratotype section and point (GSSP) of the Ladinian Stage (Middle Triassic)

- at Bagolino (Southern Alps, Northern Italy) and its implications for the Triassic time scale. *Episodes*, 28, 233–244.
- Brandner, R., Gruber, A., & Keim, L. (2007). Geologie der Westlichen Dolomiten: Von der Geburt der Neotethys im Perm zu Karbonatplattformen. *Becken Und Vulkanite Der Triassische Geo Alp*, 4, 95–121.
- Budai, T., & Vörös, A. (2006). Middle Triassic platform and basin evolution of the southern Bakony Mountains (Trandunubian Range, Hungary). *Rivista Italiana Di Paleontologia e Stratigrafia*, 112, 359–371.
- Casetta, F., Coltorti, M., & Marrocchino, E. (2018). Petrological evolution of the middle Triassic Predazzo intrusive complex, Italian Alps. *International Geology Review*, 60, 977–997.
- Castellarin, A., Lucchini, F., Rossi, P. L., Selli, L., & Simboli, G. (1988). The Middle Triassic magmatic-tectonic arc developed in the Southern Alps. *Tectonophysics*, 146, 79–89.
- Castellarin, A., Lucchini, F., Rossi, P. L., Simboli, G., Bosellini, A., & Sommariva, E. (1980). Middle Triassic magmatism in southern Alps II: A geodynamic model. *Rivista Italiana Di Paleontologia e Stratigrafia*, 85, 3–4.
- Coombs, D. S., Nakamura, Y., & Vuagnat, M. (1976). Pumpellyite-actinolite facies schist of the Taveyanne formation near Loeche, Valais, Switzerland. *Journal of Petrology*, 17, 440–447.
- Cox, K. G., Bell, J. D., & Pankhurst, R. J. (1979). *The interpretation of igneous rocks* (p. 450). George Allen and Unwin.
- Crisci, C. M., Ferrara, G., Mazzuoli, R., & Rossi, P. M. (1984). Geochemical and geochronological data on Triassic volcanism in the Southern Alps of Lombardy (Italy): Genetic implications. *Geologische Rundschau*, 73, 279–292.
- Dana, J. D., Klein, C., & Hurlbut, C. S. (1993). *Manual of mineralogy* (p. 532). Wiley.
- De Min, A., Jourdan, F., Marzoli, A., Renne, P. R., & Juračić, M. (2008). The tholeiitic magmatism of Jabuka, Vis and Brusnik Islands: A Carnian magmatism in the Adria Plate. *Rendiconti Online Società Geologica Italiana*, 2, 1–3.
- De Min, A., Velicogna, M., Ziberna, L., Chiaradia, M., Alberti, A., & Marzoli, A. (2020). Triassic magmatism in the European Southern Alps as an early phase of Pangea break-up. *Geological Magazine*, 157(11), 1800–1822.
- De Zanche, V., Gianolla, P., Mietto, P., Siorpaes, C., & Vai, P. R. (1993). Triassic sequence stratigraphy in the Dolomites (Italy). *Memorie Delle Scienze Geologie*, 45, 1–27.
- Deer, W. A., Howie, R. A., & Zussman, J. (1992). *An introduction to the rock-forming minerals* (p. 696). Longman Group Limited.
- Del Piaž, G. V., & Martin, S. (1998). Evoluzione litosferica e magmatismo nel dominio austro-sudalpino dall'orogenesi varisca al rifting permomesozoico. *Riunione estiva S.G.I., Memorie Delle Società Geologica Italiana*, 53, 43–62.
- Di Capua, A., De Rosa, R., Kereszturi, G., Le Para, E., Rosi, M., & Watt, S. F. L. (2022). Volcanically derived deposits and sequences: a unified terminological scheme for application in modern and ancient environments. *Geological Society of London Special Publications*, 520(1), 11.
- Dimitrijević, M. D. (1997). *Geology of Yugoslavia* (p. 187). Geological Institute GEMINI.
- Ellis, M., & King, G. (1991). Structural control of flank volcanism in continental rifts. *Science*, 254, 839–842.
- Fisher, R. V. (1961). Proposed classification of volcanoclastic sediments and rocks. *Geological Society of America Bulletin*, 72, 1409–1414.
- Gawlick, H.-J., Goričan, Š., Missoni, S., & Lein, R. (2012). Late Anisian platform drowning and radiolarite deposition as a consequence of the opening of the Neotethys ocean (High Karst nappe, Montenegro). *Bulletin De Société Géologique De France*, 183(4), 349–358.
- Gianolla, P., De Zanche, V., & Mietto, P. (1998). Triassic sequence stratigraphy in the Southern Alps (Northern Italy): Definition of sequences and basin evolution. *Special Publication SEPM*, 60, 719–747.
- Golub, L. J., & Brajdić, V. (1970). Eruptive and pyroclastic rocks from Vudelja and from the Bistrica brook on the northern slopes of Mt. Ivanščica (Hrvatsko Zagorje – Yugoslavia). *Zbornik radova Rudarsko-geološko-naftnog fakulteta* (30. god. rada, 1939–1969), 123–127 (in Croatian, with English abstract).
- Golub, L. J., & Vragović, M. (1975). Eruptivne stijene dalmatinskih otoka (Vis, Jabuka i Brusnik). *Acta Geologica*, 4, 341–350.
- Goričan, Š., Halamić, J., Grgasović, T., & Kolar-Jurkovšek, T. (2005). Stratigraphic evolution of Triassic arc-backarc system in northwestern Croatia. *Bulletin De Société Géologique De France*, 176, 3–22.
- Gorton, M. P., & Shandl, E. S. (2000). From continents to island arcs: A geochemical index of tectonic setting for arc-related and within-plate felsic to intermediate volcanic rocks. *Canadian Mineralogist*, 38, 1065–1073.
- Gradstein, F. M., Ogg, J. G., Schmitz, M. D., & Ogg, G. M. (2020). *Geological Time Scale 2020* (p. 1365). Elsevier.
- Grimes, C. B., Wooden, J. L., Cheadle, M. J., & John, B. E. (2015). “Fingerprinting” tectono-magmatic provenance using trace elements in igneous zircon. *Contributions to Mineralogy and Petrology*, 170, 1–26.
- Haas, J., & Budai, T. (1995). Upper Permian-Triassic facies zone in the Transdanubian Range. *Rivista Italiana Di Paleontologia e Stratigrafia*, 110, 249–266.
- Haas, J., & Kovács, S. (2001). The Dinaridic-Alpine connection – as seen from Hungary. *Acta Geologica Hungarica*, 44, 345–362.
- Haas, J., Mioč, P., Pamić, J., Tomljenović, B., Ārkai, P., Bérczi-Makk, A., Koroknai, B., Kovács, S., & R-Felgenhauer, E. (2000). Complex structural pattern of the Alpine-Dinaridic Pannonian triple junction. *International Journal of Earth Sciences*, 89, 377–389.
- Harangi, Sz., Szabó, Cs., Józsa, S., Szoldán, Zs., Árvai-Sós, E., Balla, M., & Kubovics, I. (1996). Mesozoic igneous suites in Hungary: Implications for genesis and tectonic setting in the northwestern part of Tethys. *International Geology Review*, 38, 336–360.
- Hawkesworth, C. J., Gallagher, K., Hergt, J. M., & Mcdermott, F. (1993). Trace element fractionation processes in the generation of island arc basalts. In K. G. Cox, D. P. McKenzie, & R. S. White (Eds.), *Melting and melt movement in the Earth* (pp. 179–191). Philosophical Transactions of Royal Society, Oxford University Press, A342.
- Hawkesworth, C. J., Turner, S. P., Mcdermott, F., Peate, D. W., & Van Calsteren, P. (1997). U-Th isotopes in arc magmas: Implications for element transfer from the subducted crust. *Science*, 276, 551–555.
- Hawthorne, F. C., Oberti, R., Harlow, G. E., Maresch, W. V., Martin, R. F., Schumacher, J. C., & Welch, M. D. (2012). Nomenclature of the amphibole supergroup. *American Mineralogist*, 9, 2031–2048.
- Hey, M. H. (1954). A new review of the chlorites. *Mineralogical Magazine*, 30, 277–292.
- Hnylko, O., Krobicki, M., Feldman-Olszewska, A., & Iwańczuk, J. (2015). Geology of the volcano-sedimentary complex of the Kamyanyi Potik Unit of Chyvcyn Mount (Ukrainian Carpathians): Preliminary results. *Geological Quarterly*, 59, 145–156.
- Hofmann, A. W. (1997). Mantle geochemistry: The message from oceanic volcanism. *Nature*, 385, 219–229.
- Hollocher, K., Robinson, P., Walsh, E., & Roberts, D. (2012). Geochemistry of amphibolite facies volcanics and gabbros of the Støren Nappe in extensions west and southwest of Trondheim, Western Gneiss Region, Norway: A key to correlations and paleotectonic settings. *American Journal of Science*, 312, 357–416.
- Jackson, T. A., Scott, P. W., Donovan, S. K., Pickerill, R. K., Portell, R. W., & Harper, D. A. T. (2008). The volcanoclastic turbidites of the Grand Bay Formation, Carriacou, Grenadines, Lesser Antilles. *Caribbean Journal of Science*, 44, 116–124.
- Jochum, K. P., Willbold, M., Raczek, I., Stoll, B., & Herwig, K. (2005). Chemical Characterisation of the USGS Reference Glasses GSA-1G, GSC-1G, GSD-1G, GSE-1G, BCR-2G, BHVO-2G and BIR-1G Using EPMA, ID-TIMS, ID-ICP-MS and LA-ICP-MS. *Geostandards and Geoanalytical Research*, 29, 285–302.
- Kazim, V., Berhe, S. M., Nicoletti, M., & Petrucciani, C. (1980). Evolution of the northern part of the Ethiopian rift. *Atti Dei Convegna Lincei*, 47, 275–292.
- Kinzler, R. J. (1997). Melting of mantle peridotite at pressure approaching the spinel to garnet transition: Application to mid-ocean ridge basalt petrogenesis. *Journal of Geophysical Research*, 102, 853–874.
- Knežević, V., Jovanović, V., Memović, E., & Resimović, K. (1998). Triassic magmatic rocks of Yugoslav Dinarides – in Serbia. *XIII kongres geologa Jugoslavije, Herceg Novi, Zbornik radova*. 3, 61–66 (in Serbian, with English abstract).
- Kolar-Jurkovšek, T., Jurkovšek, B., & Balini, M. (2006). Conodont zonation of the Triassic basement of the Adriatic-Dinaric carbonate platform in Mt. Svilaja (External Dinarides, Croatia). In: Purnell, M., Donoghue, P., Aldridge & R. Repetski, J. (Eds.). *International Conodont Symposium, 2006, Programme & Abstracts*, Leicester, pp. 48.
- Koppers, A. A. P. (2002). ArArCALC-software for ⁴⁰Ar/³⁹Ar age calculations. *Computers & Geosciences*, 28, 605–619.
- Kuiper, K. F., Deino, A., Hilgen, F. J., Krijgsman, W., Renne, P. R., & Wijbrans, J. R. (2008). Synchronizing rock clocks of earth history. *Science*, 320, 500–504.

- Kukoč D, Smirčić, D., Grgasović, T., Horvat, M., Belak, M., Japundžić, D., Kolar-Jurkovšek, T., Šegvič, B., Badurina, L., Vukovski, M., & Slovenec, D. (2023). Biostratigraphy and facies description of Middle Triassic rift-related volcano-sedimentary successions at the junction of the Southern Alps and the Dinarides (NW Croatia). *International Journal of Earth Sciences*, 112, 1175–1201. <https://doi.org/10.1007/s00531-023-02301-w>
- Le Bas, M. J. (1962). The role of aluminium in igneous clinopyroxene with relation to their parentage. *American Journal of Science*, 260, 267–288.
- Ludwig, K.R. (2003). *Isoplot 3.09 a geochronological toolkit for microsoft excel*. Berkeley Geochronology Center, Special Publication no. 4.
- Lugović, B., & Majer, V. (1983). Eruptivni Senjske drage (Vratnik) kod Senja (SR Hrvatska, Jugoslavija). *Geološki Vjesnik*, 36, 157–181.
- Lustrino, M., Abbas, H., Agostini, S., Gaggiati, M., Carminati, E., & Gianolla, P. (2019). Origin of Triassic magmatism of the Southern Alps (Italy): Constraints from geochemistry and Sr-Nd-Pb isotopic ratios. *Gondwana Research*, 75, 218–238.
- Marci, V., Pleteš, G., Bosak, Ž., & Šatara, D. (1991). Prvi nalaz akrecionih lapila u trijaskim naslagama kod Donjeg Pazarišta. *Geološki Vjesnik*, 43, 113–121.
- Marci, V., Ščavničar, S., & Sijarić, G. (1982). Petrogenesis of the volcanic rocks of Ivanščica Mt. (River Željeznica). *X kongres geologa Jugoslavije, Budva, Zbornik radova*, 1, 329–335.
- Marci, V., Ščavničar, S., & Sijarić, G. (1984). The new data about volcanic rocks of Ivanščica mountain. *Geološki Vjesnik*, 37, 97–104.
- Marić, L. (1976). Gabro kod Jablanice n/N u svijetlosti novih istraživanja. *Geološki Glasnik*, 21, 71–76.
- Mazzarini, F., Abebe, T., Innocenti, F., Manetti, P., & Paraschi, M. T. (1999). Geology of the Debre Zeyt area (Ethiopia) (with a geological map at scale 1:100 000). *Acta Vulcanologica*, 11, 131–141.
- McDonough, W. F., & Frey, F. A. (1989). REE in upper mantle rocks. In B. Lipin & G. R. Mckay (Eds.), *Geochemistry and mineralogy of rare earth elements* (pp. 99–145). Mineralogical Society of America.
- McKenzie, D. P., & O'Nions, R. K. (1991). Partial melt distributions from inversion of rare earth element concentrations. *Journal of Petrology*, 32, 1027–1091.
- McPhie, J., Doyle, M., & Allen, R. (1993). *Volcanic textures – a guide to the interpretation of textures in volcanic rocks* (p. 198). Centre for Ore Deposit and Exploration Studies, University of Tasmania.
- Mével, C. (1981). Occurrence of pumpellyite in hydrothermally altered basalts from Vema Fracture Zone (Mid-Atlantic Ridge). *Contributions in Mineralogy and Petrology*, 76, 386–393.
- Millot, G. (1971). *Geology of clays. weathering, sedimentology, geochemistry* (p. 429). Springer-Verlag.
- Morbiddelli, L., Nicoletti, M., Petrucciani, C., & Piccirillo, E. M. (1975). K/Ar ages of the main volcanic events (Main Ethiopian Rift from 8°10' - 9°00' lat north). In A. Pilger & A. Rosler (Eds.), *Afar depression of Ethiopia* (pp. 362–369). Schweizerbart.
- Morimoto, N. (1988). Nomenclature of pyroxenes. *Schweiz. Mineralogy and Petrology*, 68, 95–111.
- Mundil, R., Brack, P., Meier, M., Reiber, H., & Oberli, F. (1996). High resolution U-Pb dating of Middle Triassic volcanoclastics: Time-scale calibration and verification of tuning parameters for carbonate sedimentation. *Earth and Planetary Science Letters*, 141, 137–151.
- Obenholzner, J. H. (1991). Triassic volcanogenic sediments from the Southern Alps (Italy, Austria, Yugoslavia) – a contribution to the “Pietra verde” problem. *Sedimentary Geology*, 74, 147–171.
- Pamić, J. (1984). Triassic magmatism of the Dinarides in Yugoslavia. *Tectonophysics*, 109, 273–307.
- Pamić, J. (2000). Triassic Jablanica gabbro pluton in the north Hercegovina. In J. Pamić & B. Tomljenović (Eds.), *Outline of the geology of the Dinarides and South Tisia* (pp. 77–80). Springer.
- Pamić, J., & Balen, D. (2005). Interaction between Permo-Triassic rifting, magmatism and initiation of the Adriatic-Dinaridic carbonate platform (ADCP). *Acta Geologica Hungarica*, 48, 181–204.
- Pamić, J., & Tomljenović, B. (1998). Basic geological data on the Croatian part of the Mid-Transdanubian Zone as exemplified by Mt. Medvednica located along the Zagreb-Zemlen Fault Zone. *Acta Geologica Hungarica*, 41, 389–400.
- Passaglia, E., & Gottardi, G. (1973). Crystal chemistry and nomenclature of pumpellyites and jugoldites. *The Canadian Mineralogist*, 12, 219–223.
- Pearce, J. A. (1982). Trace element characteristics of lavas from destructive plate boundaries. In R. S. Thorpe (Ed.), *Andesites* (pp. 525–548). Wiley.
- Pearce, J. A. (1983). Role of the sub-continental lithosphere in magma genesis at active continental margins. In C. J. Hawkesworth & M. J. Norry (Eds.), *Continental basalts and mantle xenoliths* (pp. 230–249). Shiva.
- Pearce, J. A., Lippard, S. J., & Roberts, S. (1984). Characteristics and tectonic significance of supra-subduction zone ophiolites. *Geological Society Special Publications*, 16, 17–94.
- Pearce, J. A., & Norry, M. J. (1979). Petrogenetic Implications of Ti, Zr, Y, and Nb Variations in Volcanic Rocks. *Contributions to Mineralogy and Petrology*, 69, 33–47.
- Plank, T. (2005). Constraints from Th/La on sediment recycling at subduction zones and evolution of the continents. *Journal of Petrology*, 46, 921–994.
- Plank, T., & Langmiur, C. H. (1998). The chemical composition of subducting sediment and its consequences for the crust and mantle. *Chemical Geology*, 145, 325–394.
- Polat, A., & Hofmann, A. W. (2003). Alteration and geochemical patterns in the 3.7–3.8 Ga Isua greenstone belt, West Greenland. *Precambrian Research*, 126, 197–218.
- Polat, A., Hofmann, A. W., & Rosing, M. T. (2002). Boninite-like volcanic rocks in the 3.7–3.8 Ga Isua greenstone belt, West Greenland: Geochemical evidence for intra-oceanic subduction zone processes in the early Earth. *Chemical Geology*, 184, 231–254.
- Pouchou, J. L., & Pichoir, F. (1984). A new model for quantitative analyses. I. Application to the analysis of homogeneous samples. *La Recherche Aéropatiale*, 3, 13–38.
- Pouchou, J. L., & Pichoir, F. (1985). “PAP” (ρ - ρ -Z) correction procedure for improved quantitative microanalysis. In J. T. Armstrong (Ed.), *Microbeam analysis* (pp. 104–106). San Francisco Press.
- Rahn, M., Mullis, J., Erdelbrock, K., & Frey, M. (1994). Very low-grade metamorphism of the Tavayanne greywacke, Glarus Alps, Switzerland. *Journal of Metamorphic Geology*, 12, 625–641.
- Rollinson, H. R. (1993). *Using geochemical data: evaluation, presentation, interpretation* (p. 352). Longman.
- Saccani, E., Dilek, Y., Marroni, M., & Pandolfi, L. (2015). Continental margin ophiolites of Neotethys: remnants of Ancient Ocean-Continent Transition Zone (OCTZ) lithosphere and their geochemistry, mantle sources and melt evolution patterns. *Episodes*, 38, 230–249.
- Ščavničar, B. (1979). Sedimenti u evaporaitskom kompleksu Komiže (otok Vis). *Geološki Vjesnik*, 32, 213–227.
- Ščavničar, B., Ščavničar, S., & Šušnjara, A. (1984). The volcanic-sedimentary Middle Triassic in the Suvaja brook area (Mt. Svilaja, Outer Dinarides). *Acta Geologica*, 14, 35–82.
- Schmid, S. M., Bernoulli, D., Fügenschuh, B., Matenco, L., Scheffer, S., Schuster, R., Tischler, M., & Ustaszewski, K. (2008). The Alpine-Carpathian-Dinaridic orogenic system: Correlation and evolution of tectonic units. *Swiss Journal of Geosciences*, 101, 139–183.
- Schmid, S. M., Fügenschuh, B., Kissling, E., & Schuster, R. (2004). Tectonic map and overall architecture of the Alpine orogen. *Eclogae Geologicae Helvetiae*, 97, 93–117.
- Schmid, S. M., Fügenschuh, B., Kounov, A., Mačenco, L., Nievergelt, P., Oberhänsli, R., Pleuger, J., Schefer, S., Schuster, R., Tomljenović, B., Ustaszewski, K., & van Hinsbergen, D. J. J. (2020). Tectonic units of the Alpine collision zone between Eastern Alps and western Turkey. *Gondwana Research*, 78, 308–374.
- Šegvič, B., Slovenec, D., & Badurina, L. (2023). Major and rare earth element mineral chemistry of low-grade assemblages inform dynamics of hydrothermal ocean-floor metamorphism in the Dinaridic Neotethys. *Geological Magazine*, 160, 444–470.
- Senowbari-Daryan, B., Zühlke, R., Bechstäd, T., & Flügel, E. (1993). Anisian (Middle Triassic) Buildups of the Northern Dolomites (Italy): The recovery of reef communities after the Permian/Triassic Crisis. *Facies*, 28, 181–256.
- Shervais, J. W. (1982). Ti-V plots and petrogenesis of modern and ophiolitic lavas. *Earth and Planetary Science Letters*, 59, 101–118.
- Šimunić, An., Pikića, M., & Hećimović, I. (1982). *Osnovna geološka karta SFRJ 1:100000, list Varaždin L33–69* [Basic Geological Map of SFRY 1:100000. Varaždin sheet – in Croatian]. Institut za geološka istraživanja Zagreb, Savezni geološki zavod Beograd.
- Šimunić, An. (1992). *Geological relations of the central part of the Croatian Zagorje*. PhD Thesis, Zagreb University, 189 pp. (in Croatian, with English abstract).

- Šimunić, An., & Šimunić, Al. (1979). Petrographic composition and genesis of Triassic deposits of Ivanščica, Kalnik and Ravna gora Mt. *Geološki Vjesnik*, 32, 243–253.
- Šimunić, An., & Šimunić, Al. (1997). Triassic Deposits of Hrvatsko Zagorje. *Geologia Croatica*, 50, 243–250.
- Slovenec, D., Belak, M., Badurina, L., Horvat, M., & Šegvić, B. (2023a). Triassic evolution of the Adriatic-Dinaridic platform's continental margins – insight from rare dolerite subvolcanic intrusions in External Dinarides, Croatia. *Comptes Rendus Géoscience*, 355, 35–62.
- Slovenec, D., Horvat, M., Smirčić, D., Belak, M., Badurina, L., Kukoč, D., Grgasović, T., Byerly, K., Vukovski, M., & Šegvić, B. (2023b). On the evolution of Middle Triassic passive margins of the Greater Adria Plate: Inferences from the study of calc-alkaline and shoshonitic tuffs from NW Croatia. *Ofoliti*, 48, 31–46.
- Slovenec, D., & Šegvić, B. (2021). Middle Triassic high-K calc-alkaline effusive and pyroclastic rocks from the Zagorje-Mid-Transdanubian Zone (Mt. Kuna Gora; NW Croatia): Mineralogy, petrology, geochemistry and tectono-magmatic affinity. *Geologica Acta*, 19, 1–23.
- Slovenec, D., Šegvić, B., Halamić, J., Goričan, Š., & Zanoni, G. (2020). An ensialic volcanic arc along the northwestern edge of Palaeotethys-Insights from the Mid-Triassic volcanosedimentary succession of Ivanščica Mt. (northwestern Croatia). *Geological Journal*, 55, 4324–4351.
- Smirčić, D., Aljinović, D., Barudžija, U., & Kolar-Jurkoviček, T. (2020a). Middle Triassic syntectonic sedimentation and volcanic influence in the central part of the External Dinarides, Croatia (Velebit Mts.). *Geological Quarterly*, 64, 220–239.
- Smirčić, D., Japundžić, D., Gaberšek, N., Aljinović, D., Prlj-Šimić, N., Krizmanić, K., Barudžija, U., & Pavić, I. (2020b). First record of the upper Illyrian ammonoid subzone marker *Reitziites reitzi* in the Karst Dinarides. *Rudarsko-Geološko-Naftni Zbornik*, 35, 75–84.
- Smirčić, D., Kolar-Jurkoviček, T., Aljinović, D., Barudžija, U., Jurkoviček, B., & Hrvatović, H. (2018). Stratigraphic definition and correlation of the Middle Triassic volcanoclastic facies in the External Dinarides: Croatia and Bosnia and Herzegovina. *Journal of Earth Science*, 29, 864–878.
- Stampfli, G. M., & Borel, G. D. (2002). A plate tectonic model for the Paleozoic and Mesozoic constrained by dynamic plate boundaries and restored synthetic ocean isochrons. *Earth and Planetary Science Letters*, 196, 17–33.
- Stampfli, G. M., & Borel, G. D. (2004). The TRANSMED transects in space and time: Constraints on the paleotectonic evolution of the Mediterranean domain. In W. Cavazza, F. Roure, W. Spakman, G. M. Stampfli, & P. A. Ziegler (Eds.), *The TRANSMED Atlas: The Mediterranean Region from crust to mantle* (pp. 53–80). Springer-Verlag.
- Storck, J. C., Brack, P., Wotzlav, J. F., & Ulmer, P. (2018). Timing and evolution of Middle Triassic magmatism in the Southern Alps (Northern Italy). *Journal of the Geological Society of London*, 176, 253–268.
- Storck, J. C., Wotzlav, J. F., Karakas, Ö., Brack, P., Gerdes, A., & Ulmer, P. (2020). Hafnium isotopic record of mantle-crust interaction in an evolving continental magmatic system. *Earth and Planetary Science Letters*, 535, 116100.
- Sun, S. S., & McDonough, W. F. (1989). Chemical and isotopic systematics of oceanic basalts: implications for mantle composition and processes. *Geological Society Special Publication*, 42, 313–345.
- Sun, S. S., & Nesbitt, R. W. (1978). Geochemical regularities and genetic significance of ophiolitic basalts. *Geology*, 6, 689–693.
- Sun, S. C., Zhang, L., Li, R. H., Hao, T. W., Wang, J. Y., Li, Z. Q., Zhang, F., Zhang, X. J., & Guo, H. (2019). Process and mechanism of Gold Mineralization at the Zhengchong Gold deposit, Jiangnan Orogenic Belt: evidence from the arsenopyrite and chlorite mineral thermometers. *Minerals*, 9, 133.
- Swinden, H. S., Jenner, G. A., Fryer, B. J., Hertogen, J., & Roddick, J. C. (1990). Petrogenesis and paleotectonic history of the Wild Bight Group, an Ordovician rifted island arc in central Newfoundland. *Contributions to Mineralogy and Petrology*, 105, 219–241.
- Taylor, S. R., & McLennan, S. M. (1985). *The continental crust: Its composition and evolution* (p. 312). Blackwell Scientific Publication.
- Thirlwall, M. F., Upton, B. G. J., & Jenkins, C. (1994). Interaction between continental lithosphere and the Iceland plume – Sr–Nd–Pb isotope chemistry of Tertiary basalts, NE Greenland. *Journal of Petrology*, 35, 839–897.
- Tomljenović, B., & Csontos, L. (2001). Neogene-Quaternary structures in the border zone between Alps, Dinarides and Pannonian Basin (Hrvatsko Zagorje and Karlovac Basin, Croatia). *International Journal of Earth Sciences*, 90, 560–578.
- Tomljenović, B., Csontos, L., Márton, E., & Márton, P. (2008). Tectonic evolution of the northwestern Internal Dinarides as constrained by structures and rotation of Medvednica Mountains, North Croatia. *Geological Society London Special Publications*, 298, 145–167.
- Trubelja, F., Burgath, K. P., & Marchig, V. (2004). Triassic magmatism in the area of the Central Dinarides (Bosnia and Herzegovina): Geochemical Resolving of tectonic setting. *Geologia Croatica*, 57, 159–170.
- Uzarowicz, L., Šegvić, B., Michalik, M., & Bylina, P. (2012). The effect of hydro-chemical conditions and pH of the environment on phyllosilicate transformations in the weathering zone of pyrite-bearing schists in Wieściszowice (SW Poland). *Clay Minerals*, 47, 401–417.
- van Gelder, I. E., Matenco, L., Willingshofer, E., Tomljenović, B., Andriessen, P. A. M., Ducea, M. N., Beniast, A., & Gruici, A. (2015). The tectonic evolution of a critical segment of the Dinarides-Alps connection: Kinematic and geochronological inferences from the Medvednica Mountains, NW Croatia. *Tectonics*, 34, 1952–1978.
- van Hinsbergen, D. J. J., Torsvik, T. H., Schmid, S. M., Matenco, L. C., Maffione, M., Vissers, R. L. M., Gürer, D., & Spakman, W. (2020). Orogenic architecture of the Mediterranean region and kinematic reconstruction of its tectonic evolution since the Triassic. *Gondwana Research*, 81, 79–229.
- Velledits, F. (2004). Anisian terrestrial sediments in the Bükk Mountains (NE Hungary) and their role in the Triassic Rifting of the Vadar-Meliata branch of Neo-Tethys Ocean. *Rivista Italiana Di Paleontologia e Stratigrafia*, 110, 659–679.
- Velledits, F. (2006). Evolution of the Bükk Mountains (NE Hungary) during the Middle-Late Triassic asymmetric rifting of the Vadar-Meliata branch of the Neotethys Ocean. *International Journal of Earth Science*, 95(3), 395–375.
- Velledits, F., Lein, R., Krystyn, L., Péror, Cs., Piros, O., & Blau, J. (2017). A Reiflingi esemény hatása az Északi-Mészköalpok és az Aggteleki-hegység középső-triász fejlődésére (in Hungarian). *Földtani Közöny*, 147, 3–24.
- Vukovski, M., Kukoč, D., Grgasović, T., Fuček, L., & Slovenec, D. (2023). Evolution of eastern passive margin of Adria recorded in shallow- to deep-water successions of the transition zone between the Alps and the Dinarides (Ivanščica Mt., NW Croatia). *Facies*, 69, 18. <https://doi.org/10.1007/s10347-023-00674-7>
- Walter, M. J. (1998). Melting of garnet peridotite and the origin of komatiite and depleted lithosphere. *Journal of Petrology*, 39, 29–60.
- White, J. D. L., & Houghton, B. F. (2006). Primary volcanoclastic rocks. *Geology*, 34, 677–680.
- Wilson, M. (1989). *Igneous petrogenesis* (p. 466). Unwin Hyman Ltd.
- Wilson, M., Downes, H., & Cebria, J. M. (1995). Contrasting fractionation trends in coexisting continental alkaline magma series: Cantal, Massif Central, France. *Journal of Petrology*, 36, 1729–1753.
- Winchester, J. A., & Floyd, P. A. (1977). Geochemical discrimination of different magma series and their differentiation products using immobile elements. *Chemical Geology*, 20, 325–343.
- Wolde Gabriel, G., & Aronson, J. (1987). The Chow Bahir Rift: A “failed” rift in southern Ethiopia. *Geology*, 15, 430–433.
- Wolde Gabriel, G., Aronson, J., & Walter, R. C. (1990). Geology, geochronology, and rift basin development in the central sector of the Main Ethiopian Rift. *Geological Society of America Bulletin*, 102, 439–458.
- Wood, D. A. (1980). The application of a Th–Hf–Ta diagram to problems of tectonomagmatic classification and establishing the nature of crustal contamination of basaltic lavas of the British Tertiary volcanic province. *Earth and Planetary Science Letters*, 50, 11–30.
- Workman, R. K., & Hart, S. R. (2005). Major and trace element composition of the depleted MORB mantle (DMM). *Earth and Planetary Science Letters*, 231, 53–72.
- Zane, A., & Weiss, Z. A. (1998). Procedure for classifying rock-forming chlorites based on microprobe data. *Rendiconti Lincei*, 9, 51–56.
- Zanettin, B., Justin-Visentin, E., Nicoletti, M., & Petrucciari, C. (1978). Evolution of the Chencha escarpment and the Ganjiuli graben (Lake Abaya) in the southern Ethiopian rift. *Neues Jahrbuch Für Geologie Und Paläontologie Monatshefte*, 8, 473–490.

Publisher's Note

Springer Nature remains neutral with regard to jurisdictional claims in published maps and institutional affiliations.